

1 Estimation of NO_x and SO₂ Emissions from Sarnia, Ontario 2 using Mobile-MAX-DOAS and a NO_x-Analyzer

3 Zoe Y. W. Davis¹, Sabour Baray², Chris A. McLinden³, Aida Khanbabakhani², William Fujs²,
4 Csilla Csukat², Jerzy Deboasz⁴, Robert McLaren².

5
6 ¹Graduate Program in Earth and Space Science, York University, Toronto, M3J 1P3, Canada

7 ²Centre for Atmospheric Chemistry, York University, Toronto, M3J 1P3, Canada

8 ³Environment and Climate Change Canada, Toronto, M3H 5T4, Canada

9 ⁴Air Quality Monitoring and Assessment Unit, Ontario Ministry of the Environment, Conservation and Parks,
10 Etobicoke, M9P 3V6, Canada

11
12 *Correspondence to:* Zoe Y. W. Davis (zoeywd@yorku.ca) or R. McLaren (rmclaren@yorku.ca)

13 **Abstract.** Sarnia, ON experiences pollutant emissions disproportionate to its relatively small size. The small size of
14 the city limits traditional top-down emission estimate techniques (e.g., satellite) but a low-cost solution for emission
15 monitoring is Mobile-MAX-DOAS. Measurements were made using this technique from 21/03/2017 to 23/03/2017
16 along various driving routes to retrieve vertical column densities (VCDs) of NO₂ and SO₂ and to estimate emissions
17 of NO_x and SO₂ from the Sarnia region. A novel aspect of the current study was the installation of a NO_x analyzer in
18 the vehicle to allow real time measurement and characterization of near-surface NO_x/NO₂ ratios across the urban
19 plumes, allowing improved accuracy of NO_x emission estimates. Confidence in the use of near-surface measured
20 NO_x/NO₂ ratios for estimation of NO_x emissions was increased by relatively well-mixed boundary layer conditions.
21 These conditions were indicated by similar temporal trends in NO₂ VCDs and mixing ratios when measurements
22 were sufficiently distant from the sources. Leighton ratios within transported plumes indicated peroxy radicals were
23 likely disturbing the NO-NO₂-O₃ photostationary state through VOC oxidation. The average lower limit emission
24 estimate of NO_x from Sarnia was 1.60 ± 0.34 tonnes hr⁻¹ using local 10 m elevation wind-speed measurements. Our
25 estimates were larger than the downscaled annual 2017 NPRI reported industrial emissions of 0.9 tonnes NO_x hr⁻¹.
26 Our lower limit estimate of SO₂ emissions from Sarnia was 1.81 ± 0.83 tonnes SO₂ hr⁻¹, equal within uncertainty to
27 the 2017 NPRI downscaled value of 1.85 tonnes SO₂ hr⁻¹. Satellite-derived NO₂ VCDs over Sarnia from the Ozone
28 Monitoring Instrument (OMI) were lower than Mobile-MAX-DOAS VCDs, likely due to the large pixel size
29 relative to the city's size. The results of this study support the utility of the Mobile-MAX-DOAS method for

30 estimating NO_x and SO₂ emissions in relatively small, highly industrialized regions especially when supplemented
31 with mobile NO_x measurements.

32 **1 Introduction**

33 Differential Optical Absorption Spectroscopy (DOAS) is a remote sensing technique that quantifies tropospheric
34 trace-gases using light spectra and the unique spectral absorption cross sections of trace-gases. DOAS has been used
35 since its introduction by (Platt et al., 1979) to measure small molecular species including NO₂, SO₂, OH, BrO, NO₃,
36 NH₃, ClO and others. One advantage of the technique is the potential for simultaneous quantification of multiple
37 trace-gases (e.g., SO₂ and NO₂) (Platt et al., 2008). The Multi-Axis DOAS (MAX-DOAS) method allows sensitive
38 quantification of tropospheric pollutants by measuring scattered sunlight spectra at multiple viewing directions
39 and/or elevation angles. Spectra measured at elevation angles close to horizon-pointing have high sensitivity to
40 ground-level gases since the light paths are longer near the surface (Hönninger et al., 2004). Ground-based MAX-
41 DOAS measurements quantify total boundary layer pollution loading by determining tropospheric vertical column
42 densities (VCDs) of trace-gases. These measurements are, therefore, well suited to measuring total emissions into an
43 air mass. VCDs are independent of boundary layer height, unlike mixing ratios, and are spatially averaged
44 (horizontally and vertically) on the order of a few kilometres along the light path. Ground-based MAX-DOAS can
45 also retrieve vertical profiles of aerosol extinction and trace-gases by combining MAX-DOAS data with radiative
46 transfer modelling (Friess et al., 2006; Heckel et al., 2005; Hönninger et al., 2004; Hönninger and Platt, 2002; Irie et
47 al., 2008; Wagner et al., 2004, 2011).

48 The recently developed Mobile-MAX-DOAS technique allows measurement of trace-gas emissions from a region of
49 interest by driving the instrument around the region. The method can estimate emissions on a nearly hourly basis in
50 a region with a spatial resolution of ~1 km. Mobile MAX-DOAS has been used to estimate NO_x emissions from a
51 shipping and industrial areas (Rivera et al., 2010), power-plants (Wu et al., 2017) and cities (Ibrahim et al., 2010;
52 Shaiganfar et al., 2011, 2017), validate satellite and air quality modelled VCDs (Dragomir et al., 2015; Shaiganfar et
53 al., 2015), estimate surface NO₂ mixing ratios from NO₂ VCDs (Shaiganfar et al., 2011), and determine the
54 horizontal variability of trace-gas VCDs within satellite pixels (Wagner et al., 2010). Mobile-MAX-DOAS is a “top-
55 down” approach for quantifying real-world emissions that can be used to validate “bottom-up” emission inventories
56 (Shaiganfar et al., 2011).

57 Sarnia, Ontario, a small Canadian city, experiences pollutant emissions due to a large number of industrial chemical
58 and oil processing facilities, vehicular exhaust from the Canada-U.S.A. international border crossing, emissions
59 from large ships travelling through the St Clair River, vehicular traffic, residential heating and other anthropogenic
60 emissions from the city populace, and transnational air pollution from Ohio, Illinois and Michigan (Oiamo et al.,
61 2011). These sources contribute to increased levels of air pollutants such as NO_x , VOC's and SO_2 , which are
62 precursors of $\text{PM}_{2.5}$ and O_3 (Ministry of the Environment and Climate Change, 2015). Traditional "top-down"
63 methods for quantifying pollutant emissions from small cities (e.g., satellite monitoring, aircraft studies) are limited
64 by the small footprint. Additionally, in-situ air quality monitoring stations are limited by the bias towards near-
65 surface emissions and under-sampling of elevated emissions (Tokarek et al., 2018).

66 The Mobile-MAX-DOAS method has advantages over satellite, aircraft and in-situ techniques. Major advantages
67 over satellite techniques include 1) emissions can be estimated without the need for an a-priori vertical profile, 2)
68 accuracy of estimates can increase rather than decrease for smaller source regions, and 3) emissions may be
69 estimated many times per day. Satellite retrievals are useful for estimating "top-down" emissions on regional and
70 global scales over long periods of time (Huang et al., 2014; Kim et al., 2014; Liu et al., 2016; McLinden et al.,
71 2012). However, accuracy over small regions can be limited by insufficient pixel resolution due to horizontal
72 averaging and retrieval reliance on modelled a-priori vertical profiles that may not resolve small regions (Heckel et
73 al., 2011). Aircraft studies can quantify emissions from cities but are relatively expensive. The major advantage of
74 emissions estimates using aircraft measurements is that one can in principle fully characterize the vertical profile of
75 trace gas concentration as well as the vertical profile of wind vectors for an accurate horizontal flux measurement
76 downwind of a source (Baray et al., 2018; Gordon et al., 2015). Major advantages of the Mobile-MAX-DOAS
77 method over aircraft techniques are that 1) MAX-DOAS VCDs are already vertically integrated, reducing the
78 uncertainties due to interpolation of measurements at multiple flight altitudes and 2) MAX-DOAS studies are
79 logistically easier to conduct. However one is still left with the uncertainty of the vertical profile of wind vector
80 fields. The Mobile-MAX-DOAS technique is a solution for quantifying pollutant emissions that complements the
81 aforementioned techniques as well as in-situ monitoring, through the ability to observe localized surface based and
82 elevated emissions.

83 An uncertainty associated with MAX-DOAS and satellite methods when estimating NO_x emissions from NO_2
84 measurements is the assumptions concerning the NO_x/NO_2 relationship in the air mass, which can be variable both
85 spatially and temporally. The NO_x/NO_2 ratio is often assumed to be spatially constant, taken from literature based on
86 the season, estimated using atmospheric modelling or occasionally taken from aircraft measurements when available
87 (Rivera et al., 2010). In this study, we combined the Mobile-MAX-DOAS method with simultaneous mobile NO_x
88 measurements (NO , NO_2 , NO_x) to increase knowledge of the NO_x/NO_2 ratio in the air mass spatially and temporally
89 in order to improve the accuracy of the NO_x emission estimates obtained from NO_2 measurements. A stationary
90 modular meteorological station was deployed in the airshed provided auxiliary meteorological information, typically
91 a major source of uncertainty in Mobile-MAX-DOAS emission estimations. Hourly wind data measured at 10 m
92 elevation (agl) were also available from local, permanent monitoring stations. Vertical wind profiles were modelled
93 in high resolution (1 km x 1 km) using the version 3.9.1 Weather Research and Forecasting model (WRF) centered
94 on Sarnia (42.9745° N, 82.4066° W) in an attempt to improve upon emissions values calculated using near-surface
95 wind-speed, since wind-speeds are expected to increase with altitude. However, inter-comparison of WRF modelled
96 winds with measured near-surface winds during the study period indicated poor model performance (see
97 Supplement S2.2 for detailed results). Emissions in this study were therefore calculated using the 10 m measured
98 winds to provide lower limit estimates of the hourly emissions.

99 Our study objectives were to 1) examine the relationship between the NO_2 near-ground mixing ratios and the NO_2
100 tropospheric VCDs, 2) determine NO_x and SO_2 emissions from the city of Sarnia including industrial sources, 3)
101 determine the impact of NO_x/NO_2 variability on the accuracy of NO_x emission estimates, and 4) examine OMI
102 satellite intrapixel NO_2 homogeneity. This study aims to demonstrate the utility of this method for determining
103 trace-gas emissions and monitoring pollutant transportation in Sarnia and similar urban/industrial areas.

104 **2 Experimental**

105 **2.1 Location and Instruments**

106 Measurements were conducted in and around the city of Sarnia (42.9745° N, 82.4066° W), located in southwestern
107 Ontario, Canada at the border with Port Huron, MI, U.S.A (Fig.1). The routes driven in the vehicle aimed to capture
108 major NO_x and SO_2 emission sources at different distances downwind, dependent on the prevailing wind conditions.

109 The metro area has a population of ~72,000 (2016 census) and an area of ~165 km². Sources of air pollution in this
110 region include emissions from large ships, anthropogenic emissions from the cities of Sarnia and Port Huron,
111 transport from the cities of Windsor and Detroit (60 km SW), the St Clair and Belle River power-plants (20 km
112 SSW), oil refineries and chemical industry in Sarnia, and the cross-border traffic between Canada and the U.S.A.
113 along Highway 402. Emissions from ships along the St. Clair River, normally a major source, were absent during
114 the time of our study since the canal had not opened for the season.

115 A mini-MAX-DOAS instrument (Hoffmann Messtechnik GmbH) measured scattered sunlight spectra during three
116 days: 21/03/2017 to 23/03/2017 (“Days 1 to 3”) while mounted on top of a car in a backwards pointing direction.
117 The instrument has a sealed metal box containing entrance optics, UV fibre coupled spectrometer and electronics.
118 Incident light is focused on a cylindrical quartz lens (focal length = 40 mm) into a quartz fibre optic that transmits
119 light into the spectrometer (OceanOptics USB2000) with a field of view approximately 0.6°. The spectrometer has a
120 spectral range of 290-433 nm, a 50µm wide entrance slit yielding a spectral resolution was ~0.6 nm. The
121 spectrometer is cooled and stabilized by a Peltier cooler. Spectrometer data was transferred to a laptop computer via
122 USB cable. Spectra were obtained with an integration time of ~1 minute with the continuously repeating sequence
123 of viewing elevation angles (30°, 30°, 30°, 30°, 40°, 90°). The vehicle was driven at a low but safe target speed of 50
124 km hr⁻¹ when possible to provide a spatial resolution of ~ 1 km, but speeds were occasionally up to 80 km hr⁻¹ when
125 necessary. Tropospheric VCDs were estimated from the 30° and 40° elevation angle spectra. The 40° spectra allow
126 verification that aerosol levels were sufficiently low to determine VCDs without radiative transfer modelling since
127 VCDs obtained from both angles should be equal within ±15% under low to moderate aerosol loading conditions
128 (Wagner et al., 2010). The cool temperatures in March aided in this as secondary organic aerosol loading tends to be
129 low in this season due to an absence of biogenic emissions.

130 A Model 42 chemiluminescence NO-NO₂-NO_x Analyzer (Thermo Environmental Instruments Inc.) mounted in the
131 vehicle measured NO, NO₂, and NO_x (NO+NO₂) near-surface mixing ratios. A PTFE inlet tube (5m length and
132 ID=1/4”) was mounted above the front vehicle window on the passenger side (~1.5 m above ground). The
133 instrument alternately recorded average NO-NO₂-NO_x mixing ratios with a temporal resolution of 1 minute. Most of
134 the routes were driven downwind of Sarnia on rural remote roads with little to no traffic such that NO_x emissions
135 from other vehicles were not a concern. When NO_x from other vehicles was a potential concern, data was filtered

136 out via careful note taking. The instrument indirectly measures NO₂ by subtracting the NO chemiluminescence
137 signal obtained when air bypasses a heated Molybdenum (Mo) convertor from the successive total NO_x
138 chemiluminescence signal obtained when air passes over the Mo-convertor. The NO_x analyzer can overestimate NO_x
139 and NO₂ due to the potential contribution of other non-NO_x reactive nitrogen oxides (NO_z) other than NO₂ that can
140 also be reduced to NO by the Mo converter (HNO₃, HONO, organic nitrates, etc.), leading to an overestimation
141 (Dunlea et al., 2007). Since this overestimation is more important in low NO_x regions, only data with NO_x mixing
142 ratios > 3 ppb were used. Mixing ratios of <3ppb NO₂ were only measured outside of plume-impacted regions when
143 NO₂ VCDs were also low. The potential error in NO_x/NO₂ ratios is addressed further in section 3.2. NO_x mixing
144 ratios can also have an error when successive NO and NO_x measurements occurred in areas with a significant
145 temporal gradient in the NO_x emissions. Such gradients were seen due to passing vehicles or localized industrial
146 NO_x plumes. These data were removed based on records of passing vehicles and other local near-surface sources or
147 whenever the NO₂ mixing ratios were reported as negative. Few data points were removed because the routes driven
148 were primarily rural roads with extremely low traffic density.

149 Aura satellite Ozone Monitoring Instrument (OMI) data were obtained for overpasses of the Sarnia, Ontario area for
150 Days 1 and 3. Tropospheric NO₂ VCDs are the NASA Standard Product Version 3.0 with AMFs recalculated using
151 the Environment and Climate Change Canada regional air quality forecast model GEM-MACH. The OMI
152 instrument makes UV-vis solar backscatter radiation measurements with a spatial resolution of 13x24 km² at nadir
153 and up to 28x150 km² at swath edges (Ialongo et al., 2014). The NO₂ detection limit of OMI is 5×10¹⁴ molec cm⁻²
154 (Ialongo et al., 2016). The OMI data used were screened for row anomalies that have affected OMI data since June
155 2007 (Boersma et al., 2007).

156 **2.2 MAX-DOAS Determination of VCDs**

157 Trace-gas Differential Slant Column Densities (DSCDs) were obtained using the DOAS technique (Platt et al.,
158 2008) with the spectral fitting range of 410-435 nm for NO₂ at 293 K and 307.5-318 nm for SO₂ at 293 K. All trace-
159 gas cross-sections used were from (Bogumil et al., 2003). For both gases, spectral fits also included a Fraunhofer
160 Reference Spectrum (FRS), Ring Spectrum created from the FRS, O₃ cross-sections at 223 K and 297 K, and a
161 third-order polynomial. The NO₂ cross-section was included in the SO₂ fits. Formaldehyde (HCHO) was not
162 included in the fits for SO₂ as it was expected to be very low, and did not affect the residuals for the SO₂ fits. NO₂

163 DSCDs from Day 1 were fit against a single, same-day FRS obtained in a low-pollutant region near solar-noon time.
 164 These DSCDs were corrected for SCD(FRS) and SCD(Solar Zenith Angle (SZA)) contributions using the $DSCD_{offset}$
 165 method (Wagner et al., 2010). The SCD(FRS) is the constant tropospheric trace-gas SCD component present in the
 166 FRS that causes an underestimation in the fitted DSCD. The SCD(SZA) is the difference between the stratospheric
 167 trace-gas component in the FRS and the measured non-zenith spectra. SCD(SZA) varies over time of day (t_i),
 168 maximizing overestimation in the DSCD early and late in the day. The sum of SCD(FRS) and SCD(SZA) is
 169 collectively known as the $DSCD_{offset}$. The $DSCD_{offset}(t_i)$ function was estimated by fitting a second order
 170 polynomial to multiple pairs of DSCDs of spectra (non-zenith and zenith from the same sequence), described in
 171 detail in (Wagner et al., 2010).

172 The $DSCD_{offset}$ polynomial is most accurate when successive spectra in each sequence observe similar mixing ratio
 173 fields, and measurements obtained many data-points over most of the daylight hours. However, routes on Days 2
 174 and 3 included driving in and out of both high and low NO_x regions within short time-periods and thus met neither
 175 of the requirements listed above for the $DSCD_{offset}$ method. On these days, a second method was used where NO_2
 176 DSCDs were fit against an FRS spectrum obtained close in time (<25 minutes) along each respective route in a low-
 177 pollutant region. The impacts of SCD(FRS) and SCD(SZA) on the retrieved DSCDs can be assumed to be negligible
 178 since each FRS was from a low-pollutant area and obtained close in time, respectively. This method was also used
 179 for the Day 1 SO_2 route since limited data were available but included background SO_2 measurements close in time.
 180 For all routes trace-gas tropospheric VCDs were determined by assuming a single scattering event occurred for each
 181 photon such that the air-mass factor (AMF) depended only on the viewing elevation angle, α , $AMF_{trop}(\alpha) \approx \frac{1}{\sin(\alpha)}$
 182 (Brinkma et al., 2008; Wagner et al., 2010). This “geometric approximation” is most valid under low to moderate
 183 aerosol loading and has been shown to deviate from the typically more accurate radiative transfer modelling by up to
 184 $\pm 20\%$ under moderate aerosol loading (Shaiganfar et al., 2011). Day 1 VCDs were calculated following Eq. (1):

$$VCD_{trop} = \frac{DSCD_{meas}(\alpha, t_i) + DSCD_{offset}(t_i)}{\frac{1}{\sin(\alpha, t_i)}} \quad (1)$$

185 Days 2 and 3 NO_x and Day 1 SO_2 VCDs were calculated following Eq. (2):

$$VCD_{trop} \approx \frac{DSCD_{meas}(\alpha, t_i)}{\frac{1}{\sin(\alpha, t_i)}} \quad (2)$$

186 The VCD of SO₂ was above detection limit on only two occasions in this study (both on Day 1), in contrast to NO₂.
 187 The detection limit of SO₂ is higher than NO₂ for several reasons, first, it's differential cross section is less than that
 188 of NO₂ and, second, its absorption features are in the UV wavelength region where scattered sunlight intensity is
 189 much less than that in the visible region. The fast measurements required in mobile DOAS also allow limited
 190 averaging of spectra compared to stationary measurements (Davis et al., 2019), where detection of industrial SO₂
 191 plumes is easier. Therefore, SO₂ DSCDs were only above detection limits for Day 1 Routes 3 & 4 when the light
 192 levels were highest, and the vehicle observed the combined plumes of the largest SO₂ sources in the area.

193 **2.3 Estimating Trace-gas Emissions from MAX-DOAS VCDs**

194 Trace-gas emission estimates were calculated following a flux integral approximation Eq. (3):

$$E = \left[\sum_i (VCD_{outflow,i} - VCD_{influx,i}) w_i \sin(\beta_i) ds \right] \frac{MW}{Av} \quad (3)$$

195 where VCD_{outflow,i} is the VCD measured at position i along the route s for distance ds, VCD_{influx,i} is either the
 196 measured influx values or the estimated background VCD value, w_i is the wind-speed, β_i is the angle between the
 197 driving direction and the wind-direction, MW is the molecular weight of the target gas, and Av is Avogadro's
 198 number. Transect routes were designed to observe both within and beyond emission impacted areas since routes
 199 encircling the emission sources were often not possible. Flux integrals were calculated using portions of the
 200 transects impacted only by the Sarnia urban/industrial plume in cases where plumes from other sources impacted the
 201 transect (i.e., Day 1; U.S.A. power-plant plumes). In these cases, the end-points of integration were chosen
 202 judiciously where NO₂ VCDs and surface mixing ratios decreased to a minimum at the edge of the Sarnia emissions.
 203 This method assumes that the wind-field and trace-gas emission rates are constant during the time required to drive a
 204 route. The validity of this assumption improves with decreased time for driving route completion. The Sarnia region
 205 is ideal for this method since a small geographical area contains the majority of the emissions and is surrounded on
 206 three sides by rural regions with low anthropogenic emissions.

207 A potential source of uncertainty in Mobile-MAX-DOAS emission estimates is variation in the wind fields and/or
 208 source emission rates while driving (Ibrahim et al., 2010; Wu et al., 2017). Previous studies have estimated wind-
 209 fields from local meteorology stations (Ibrahim et al., 2010), meteorological models (Shabbir et al., 2016;
 210 Shaiganfar et al., 2011, 2017) or LIDAR measurements (Wu et al., 2017). In our study, wind field information was

211 obtained from a Modular Weather Station (Nova Lynx 110-WS-25DL-N) we deployed near one of the driving
212 routes at (42.8148°, -82.2381°) (Fig. 1) and from meteorological ground stations in the area (Fig. 1, Table S1, Fig.
213 S1). The modular weather station measured wind-speed and direction, temperature, relative humidity, and
214 barometric pressure at 2 m above the surface every 30 seconds. Wind data was available from the Sarnia-Lambton
215 Environmental Association (SLEA) LaSalle Road (42.911330°, -82.379900°) and Moore Line (42.83954°, -
216 82.4208°) meteorological stations that are located near the driving routes (Fig. 1). These stations were surrounded
217 by fallow, flat farm-land for at least 4 km on each side and thus should reflect total boundary layer for plumes
218 transported away from the city more than the urban stations (Fig. S1). The hourly wind-direction data from the
219 modular and permanent stations exhibited similar values ($\pm 10^\circ$) and trends on Day 1 (Fig. S2). Wind-directions for
220 Days 2 and 3 were obtained by determining the angle of a vector drawn between the geographical locations of the
221 maximum NO₂ VCD enhancements and the industrial facilities expected to have emitted the plumes. These map-
222 determined wind-directions were consistent ($\pm 10^\circ$) with the data from the station(s) closest to the driving route.
223 Comparison of wind-speed data on Days 2 and 3 was not possible due to a technical issue with the modular weather
224 station on these days.

225 The NO₂ VCD influx (background VCD) was estimated on Day 1 since measurement was impossible along the
226 western border of Sarnia due to the road configuration and proximity of industrial emissions. A NO₂ VCD_{influx} =
227 2×10^{15} molec cm⁻² was estimated based on OMI satellite VCDs of $\sim 1.5\text{-}3.5 \times 10^{15}$ molec cm⁻² from the area east of
228 Sarnia that are expected to be similar to the NO₂ regime west of Sarnia. These pixels are expected to be unaffected
229 by other sources. The influx would be expected to be impacted by vehicular and residential emissions from the small
230 city of Port Huron, U.S.A., on the west side of the St Clair River (Fig. 1), which has limited industry but a moderate
231 level of commercial vehicle activity due to border-crossings. A first order emission estimate of vehicular NO_x
232 emissions from Port Huron from daily reported traffic counts results in an upper limit of NO₂ influx VCD of
233 $\sim 1 \times 10^{15}$ molec cm⁻² (see Supplement S4). True influx would vary along the length of the measurement transect,
234 depending on what sources are upwind of the location. Halla et al. (2011) measured NO₂ tropospheric VCDs using
235 MAX-DOAS in a similar region approximately 70 km south-east of Sarnia. The observed NO₂ VCDs in that study
236 ranged from 0.01 to 1.25×10^{16} molec cm⁻² with a median value of 2×10^{15} molec cm⁻², which is expected to be
237 representative of background NO₂ columns in this region. The highest VCD in that study was attributed to the
238 transport of industrial emissions from the Sarnia area and/or from Detroit, MI to the northwest and west of the site

239 respectively (Halla et al., 2011). Based on the range of VCDs from literature, vehicular emission estimates and
240 satellite measurements, a background VCD of 2×10^{15} molec cm^{-2} is a reasonable estimate, and emissions sensitivity
241 tests were conducted using influx VCDs of $0.5\text{-}3 \times 10^{15}$ molec cm^{-2} (Supplement S5). In contrast, the NO_2 $\text{VCD}_{\text{influx}}$
242 on Days 2 and 3 and SO_2 $\text{VCD}_{\text{influx}}$ on Day 1 were determined from the average VCDs measured in the low-
243 pollution area of each transect.

244 2.3.1 Determination of NO_x emission estimates from NO_2 measurements

245 NO_x emissions were estimated using Equation 4 from the NO_2 flux integral and the average NO_x/NO_2 ratio ($\text{NO}_x > 3$
246 ppb) measured by the NO_x -analyzer along the route. The emission values were then corrected for expected NO_x loss
247 during transport using a NO_x lifetime, τ . NO_x emission estimates were calculated as follows:

$$E_{\text{NO}_x} = E_{\text{NO}_2} * \frac{\overline{\text{NO}_x}}{\text{NO}_2} * e^{\left(\frac{y/w}{\tau}\right)} \quad (4)$$

248 where τ is NO_x lifetime, w is wind-speed, and y is the distance between the NO_x source and the measurement
249 location. For routes where individual NO_x/NO_2 ratios deviated significantly from the route average, the NO_x
250 emission estimates were calculated by applying 1) the route-averaged NO_x/NO_2 ratio and 2) individual NO_x/NO_2
251 ratios associated with each NO_2 VCD point by point. Multiple factors determine NO_x lifetime in a plume. A NO_x
252 lifetime of 6 hours was used in this study based on considerations given in section 3.3. A sensitivity analysis was
253 performed varying the lifetimes between 4-8 hours (Supplement S7). The conversion factors used to calculate NO_x
254 emissions for each route can be found in Table S8. The NO_x/NO_2 ratios are more fully addressed in Section 3.2 and
255 the NO_x lifetime is addressed in Section 3.3.

256 3 Results & Discussion

257 3.1 Relationship between NO_2 VCDs & NO - NO_2 - NO_x Analyzer Measurements

258 Figure 2 shows that enhancements in NO_2 VCDs downwind of Sarnia were generally associated with NO_2 surface
259 mixing ratios enhancements during Days 1 and 2. This suggests that pollution from Sarnia was well-mixed within
260 the boundary layer at the measurement locations, typically 14-23 km downwind of sources (Figs. 3 & 4). However,
261 the ratio of NO_2 VCD to NO_2 mixing ratio was sometimes variable even during relatively short time periods when

262 the boundary layer height was expected to be constant (Fig. 2a). This variability was probably due to the presence of
263 multiple NO_x plumes that had originated from sources with different heights (i.e., stacks and surface sources) and
264 emission rates.

265 In contrast to Days 1 and 2, NO₂ VCD enhancements on Day 3 were not consistently associated with NO₂ surface
266 mixing ratio enhancements (Figs. 5 & 6). A large surface enhancement (NO_x=22 ppb) was observed at the location
267 of the VCD NO₂ enhancements ($\sim 2.5 \times 10^{16}$ molec cm⁻²) associated with the NOVA Chemicals industrial plume on
268 route 2 (Figs. 5b & 6b) but not on route 1 (Fig. 5a & 6a). This discrepancy is likely due to the closer proximity of
269 the driving route to the source compared with Day 1, combined with limited vertical mixing of the plume. The
270 relatively long sampling time of the NO_x analyzer with a relatively fast driving speed on this route may also have led
271 to an underestimation of the true NO_x values for this localized plume.

272 3.2 NO_x/NO₂ Ratios

273 The NO_x/NO₂ ratio is necessary to estimate NO_x emissions from the source, given measurements of NO₂ VCD's
274 (Eq. 4). Ratios of NO_x/NO₂ (Table 2) measured along the routes on Days 1 and 3 were within 20% of the route-
275 averaged value with a relative standard deviation of less than 12%. NO_x/NO₂ ratios tended to increase at locations
276 associated with transported plumes' centerlines, as expected due to an increase in NO emissions from the sources
277 (see Fig. 7), and exhibited the greatest variability in air-masses affected by sources with different altitudes and
278 emission rates. Day 1, route 1 exhibited variable NO_x/NO₂ ratios due to emissions from the power-plants across the
279 river in Michigan, residential and vehicular traffic, and industrial emissions (Figs. 3a & 7).

280 Potential errors may exist in the NO_x/NO₂ ratio due to the presence of other NO_z species in the air mass (e.g., HNO₃,
281 HONO, NO₃, N₂O₅, organic nitrates, etc.) that are also converted to NO by the Mo-converter in addition to NO₂
282 (Dunlea et al., 2007). However, these errors are smaller than might be expected due to the presence of the error in
283 both the numerator and the denominator of the ratio, $NO_x/NO_2 = (NO+NO_2)/NO_2$, thus partially offsetting each
284 other. For example, at an apparent NO_x/NO₂ ratio of 1.40 (average in Table 2), a 10% and 30% error in the reported
285 NO₂ due the presence of other NO_z species gives rise to errors of only -2.6% and -6.6% in the measured NO_x/NO₂
286 ratio respectively. Mathematically, the error in the NO_x/NO₂ ratio gets larger as the percentage of NO in the total
287 NO_x increases. However, since most of the interfering NO_z species are generated photochemically, or only at night

288 (NO₃, N₂O₅) increasing with reaction time and distance away from the source, the percentage of interfering species
289 is smaller at higher values of total NO and NO_x. Under significantly intense photochemical conditions in the
290 MCMA-2003 field campaign in Mexico, the interference in the chemiluminescence monitors resulted in average
291 NO₂ concentrations being 22% higher than those determined from spectroscopic measurements (Dunlea et al.,
292 2007), which would give rise to an error in the NO_x/NO₂ ratio of <5%. In the current study we estimate that the
293 resultant negative bias in the measured NO_x/NO₂ ratio does not exceed -5% for several reasons; i) we filter out low
294 NO_x data (<3ppb), ii) the emission integral is dominated by regions with high NO_x that are spatially and temporally
295 close to the sources and, iii) photochemistry was reduced during this spring campaign. The uncertainty that arises
296 from potential errors in the NO_x/NO₂ ratio is insignificant compared to other errors (see Supplemental Table S9). It
297 is also worth noting that NO₂ measurements by the NO_x analyzer are not directly used for the calculation of
298 emissions; only the NO_x/NO₂ ratio is used.

299 Previous Mobile-MAX-DOAS studies have relied on literature estimates of the NO_x/NO₂ ratio (Shabbir et al., 2016;
300 Shaiganfar et al., 2011) or estimated the ratio from a Leighton ratio calculated using local air quality station data
301 (Ibrahim et al., 2010). In regions with many pollutant sources throughout (e.g., megacities), this ratio is expected to
302 be horizontally and vertically inhomogeneous. The ratio can therefore be challenging to estimate and can increase
303 the uncertainty of the NO_x emission estimate. Estimation of NO_x/NO₂ ratios from near-surface monitoring stations
304 can be problematic because the ratios are applied to a VCD but may reflect only local emissions (e.g., nearby
305 vehicular exhaust) rather than the total boundary layer. In this study, NO_x data impacted by local emissions were
306 removed. Also, the Sarnia emissions were expected to be well mixed to the surface since most of the transects were
307 driven sufficiently far from the sources. Therefore, the near-surface NO_x/NO₂ ratios should be representative for the
308 altitude range of the dispersed NO_x plume(s). This hypothesis is supported by the similarity between the NO₂
309 surface and VCD temporal trends during the study, especially on Days 1 and 2 (Fig. 2).

310 **3.3 NO_x Lifetime**

311 Various lifetimes of NO_x, τ , have been used in previous mobile MAX-DOAS studies for the calculation of NO_x
312 emissions from NO₂ measurements: 6 hr in Germany (Ibrahim et al., 2010), 5 hr in Delhi (Shaiganfar, 2011), 5 hr in
313 China (Wu et al., 2017) and 3 hr summer – 12 hr winter in Paris (Shaiganfar, 2017). In Beirle et al. (2011), the
314 daytime lifetime of NO_x was quantified by analyzing the downwind patterns of NO₂ measured by satellite

315 instruments and shown to vary from ~4 hr in low to mid-latitude locations (e.g., Riyadh, Saudi Arabia) to ~8hr in
316 northern locations in wintertime (e.g., Moscow, Russia). In a follow up study, Valin et al (2013) showed that one
317 cannot assume that τ is independent of wind speed and derived values of τ from the satellite observations over
318 Riyadh to be 5.5hr to 8 hr, corresponding to OH levels of $5-8 \times 10^6$ molec cm^{-3} at high and low wind speeds.

319 Multiple factors determine NO_x lifetime in a plume, including season (e.g., insolation) (Liu et al., 2016), latitude,
320 wind-driven dilution (Nunnermacker et al., 2000; Valin et al., 2013), NO_x emission rate and initial dilution
321 (Nunnermacker et al., 2000), temperature, hydroxyl radical levels (OH) and precursors to OH including O_3 , H_2O ,
322 and HONO. Very importantly, the daytime lifetime of NO_x is a nonlinear function of the NO_x concentration itself,
323 having longer lifetimes at high and low concentrations with the shortest lifetimes at intermediate NO_x concentrations
324 due to the impact on OH levels in a non-linear feedback on its own lifetime (Valin et al., 2013). The NO_x lifetime is
325 ultimately dependent on the OH levels since this dictates the loss rate of NO_2 to its terminal sink ($\text{NO}_2 + \text{OH} \rightarrow$
326 HNO_3). However the presence of VOC's in the urban plume, which are catalytically oxidized forming O_3 in the
327 presence of NO_x and HO_x ($\text{OH} + \text{HO}_2$), can decrease the NO_x lifetime due to their acceleration of the conversion of
328 NO to NO_2 via peroxy radical reactions ($\text{RO}_2 + \text{NO} \rightarrow \text{NO}_2 + \text{RO}$). Therefore, NO_x lifetimes can vary both spatially
329 and temporally (Liu et al., 2016), even within the same plume (Valin et al., 2013). Underestimation of the true NO_x
330 lifetime leads to overestimation of the NO_x emissions, while an overestimate leads to an underestimation of the
331 emissions.

332 While photolysis of HONO is often the major source of OH in the morning boundary layer (Platt et al., 1980; Alicke
333 et al., 2002), midday production of OH via photolysis of O_3 and subsequent reaction of $\text{O}(^1\text{D})$ with water is
334 frequently the dominant source of OH. Assuming $\text{O}(^1\text{D})$ is in steady-state, it can be shown that when ozone
335 photolysis is the main source of OH, the product of the mixing ratios of H_2O and O_3 is proportional to the
336 production rate of OH. In this study, the $[\text{H}_2\text{O}] * [\text{O}_3]$ product was calculated using surrounding station measurements
337 (see Supplement S8.1). The $[\text{H}_2\text{O}] * [\text{O}_3]$ product indicates that mid-day OH production under the spring-conditions
338 for Days 1 and 2 is only 10-25% of the expected OH production under warmer more humid summer-conditions,
339 presuming that O_3 photolysis predominates. This might suggest OH levels were lower in our study than during
340 summer, and hence NO_x lifetimes longer. However we assume this with caution as the HONO production is not
341 known nor are the loss rates of OH.

342 As mentioned, the presence of VOC's can decrease the lifetime of NO_x under conditions where NO_x is sufficiently
343 high to dominate the peroxy radical reaction path. To test for the presence of VOC's in the plumes (in the absence of
344 measurements), Leighton ratios, ϕ (Leighton, 1961), were calculated at locations of maximum NO₂ VCD associated
345 with Sarnia plumes. Leighton ratios were calculated following Eq. (5) (see Supplement S8.2 for details):

$$\phi = \frac{j_{NO_2}[NO_2]}{k_8[NO][O_3]} \quad (5)$$

346 where j_{NO_2} is the NO₂ photolysis rate, k_8 is the temperature-dependent rate constant for the reaction between NO and
347 O₃. Leighton ratios equal to 1.0 indicate that NO, NO₂ and O₃ are in steady state with no significant interference
348 from other species, while ratios of ϕ greater than 1.0 imply the role of other peroxy radical species (e.g., RO₂, HO₂)
349 in the conversion of NO to NO₂ (Pitts and Finlayson-Pitts, 2000). The NO₂/NO ratios were obtained from the NO_x
350 analyzer measurements, O₃ mixing ratios were obtained from local monitoring stations during the same daytime
351 periods as the transects. Values of j_{NO_2} were estimated using SLEA Moore Line station solar irradiance data (Fig. 1;
352 Table S1) and solar zenith angle following the method in Wiegand and Bofinger (2000).

353 Table 3 shows Leighton ratios calculated at the locations of maximum NO₂ VCD enhancements. Calculated
354 Leighton ratios were significantly greater than 1 ($\phi = 1.7$ - 2.3) at peak NO_x locations on Day 1 (Table 3). Even if we
355 consider a potential bias of + 20% in the NO₂ measurements by the NO_x analyzer for reasons outlined in Section 3.2
356 (highly unlikely in a fresh NO_x plume), a +20% bias in the Leighton ratio would still give ($\phi = 1.4$ - 1.9). We interpret
357 this as an indication that significant levels of peroxy radicals were present in the plume, presumably from VOC
358 oxidation by the OH radical. This is consistent with high VOC emissions from the petrochemical facilities in Sarnia,
359 with emission rates >300 tonnes yr⁻¹ each for four of the top six industrial NO_x emitters in Sarnia (Environment and
360 Climate Change Canada, 2018d). The Day 2 Leighton ratio of less than 1.0 in Table 3 suggests a relatively fresh
361 plume (only 4 km downwind of a facility) that had not come to photo-stationary state.

362 Thus we have indications that OH production may be lower than summer time leading to longer NO_x lifetimes and
363 we have indications that VOC oxidation in the plume may be significant leading to shorter NO_x lifetimes than air
364 masses where the photo-stationary state in NO_x is valid. Without further information, we have opted to assume a
365 central NO_x lifetime assume of ~ 6 hr. Sensitivity calculations were conducted for NO_x emission estimates using a

366 range of lifetimes of 4-8 hours (Supplement S7). Varying the lifetime from ± 2 hours changed the emission estimates
367 by <15% for all routes except for Day 1 route 1 due to low wind-speeds during that route (30% change).

368 For the calculation of SO₂ emissions, SO₂ was assumed to have a sufficiently long lifetime in the boundary layer so
369 as to be conserved between the emission and measurement location. Note that cloud processing of SO₂ was assumed
370 to be negligible since SO₂ measurements were completed on a mostly cloud-free day.

371 **3.4 Emission Estimates**

372

373 **3.4.1 Emission Estimates of Sarnia**

374 The VCDs measured are shown in Fig. 3-6 while the NO_x emissions calculated using Eqs. (3) and (4) are shown in
375 Table 4. The values of VCD_{influx} required for the calculations were typically determined from measurements of VCD
376 in low pollution transect areas. However, the VCD_{influx} on Day 2 was not determined in this way since these DSCDs
377 were close to zero within error (Figs. 2 & 4). The VCD_{influx} is expected to be low on Day 2 because the north wind-
378 direction indicates that the air-masses originated from over Lake Huron. These low values were probably due to low
379 light levels during measurement, insufficiently long integration times (low signal to noise ratio) and NO₂
380 background VCD values below the instrument's limit of detection. A low value of VCD_{influx} = $0.5(\pm 0.5) \times 10^{15}$ molec
381 cm⁻² was therefore assumed.

382 The emissions were calculated in two ways i) using a route-average NO_x/NO₂ ratio value for each route estimate and
383 ii) using individual NO_x/NO₂ ratios co-located with each VCD measurement. For Day 1 route, the route average
384 NO_x/NO₂ ratio was 1.53 ± 0.12 ppb ppb⁻¹ with the difference between the calculated emission rates using the two
385 methods being only 3%. Day 1 transects 2-4 exhibited small variability in NO_x/NO₂ (Table 2) and the variation in
386 the NO_x/NO₂ ratio impacted emission estimates by less than 5%.

387 However, the difference between emission estimates calculated using individual NO_x/NO₂ ratios versus a route-
388 averaged value can be non-trivial, as observed with the Day 2 route 1. Day 2 had consistent northerly wind
389 conditions, and east-west transects were driven south of Sarnia to capture the urban plume and background regions
390 to the east (Fig. 4). The resultant Sarnia NO_x emission using the first method is consistent with the first three Day 1
391 emission estimates but the application of the second method (individual NO_x/NO₂ ratios collocated with each VCD)

392 increased the emission estimate by ~50% (Table 4 and Fig. 8). The NO_x/NO_2 ratio was generally consistent with the
393 averaged value of 1.3 (maximum NO_x/NO_2 removed) but increased to 3 in the region of maximum NO_2 VCD
394 enhancements 7 km south of the NOVA Chemicals facility (Table 2). The calculated Leighton ratio for this peak
395 NO_x/NO_2 ratio location is less than 1 (see 3.4.2 and Table 3). The Leighton ratio suggests the plume from the
396 NOVA Chemical facility had significant NO that had not had sufficient time to come to a photostationary state. The
397 emission estimate using individual NO_x/NO_2 ratios is considered the more accurate value for this route compared to
398 the emission value calculated using the route-averaged ratio.

399 The importance of measuring the local NO_x/NO_2 ratio is also illustrated by observing variation of the ratio due to the
400 impact of the Michigan power-plants' plume, apparent in the Day 1 route 1 East-West transect (Fig. 3a). The
401 NO_x/NO_2 ratio along this transect increased to ~1.7 (Fig. 7), higher than the maximum NO_x/NO_2 ratio observed in
402 the North-South transect downwind of Sarnia. A higher ratio is somewhat unexpected because the distance between
403 the source and receptor measurement for the power plant source was greater than the source-receptor distance for the
404 Sarnia sources. Thus, the power-plant plume would have been expected to be more aged, but the results suggest that
405 the power-plants' plumes had a slower conversion of NO to NO_2 perhaps due to higher initial mixing ratios of NO_x
406 (Nunnermacker et al., 2000). Very high NO mixing ratios in a power plant plume (i.e., > 40ppb) could completely
407 titrate the ambient O_3 in the air entrained into the plume, an observation previously seen in power plant plumes
408 (Brown et al., 2012).

409 The East-West transect appears to have captured approximately half of the power-plants' plume since the NO_2
410 VCDs and the NO_2 mixing ratios increase from background to a plateau at a maximum (Fig. 2a). A preliminary
411 estimation of the NO_x and SO_2 emissions from the power-plants can be determined by scaling up the flux integral
412 from the appropriate section of the East-West transect by a factor of two. While this is highly uncertain, we do this
413 to make a first order estimate of the power plant plumes on the US side of the border. In this case, we have used
414 $\text{VCD}_{\text{influx}} = 2\text{-}3 \times 10^{15}$ molec cm^{-2} for NO_x and zero for SO_2 since the background region SO_2 DSCDs were at or
415 below detection limits. The NO_x estimate used individual NO_x/NO_2 ratios because the NO_x/NO_2 ratio was
416 significantly higher in the plume than outside the plume. This illustrates the importance of in-situ instruments of
417 NO_x/NO_2 , especially when close to the source where plume NO_x/NO_2 ratios can be variable (Valin et al., 2013).
418 Given the above assumptions, a tentative first order estimate of the total emissions from the power plants are 0.31-

419 0.46 tonnes $\text{NO}_x \text{ hr}^{-1}$ and 0.77 tonnes $\text{SO}_2 \text{ hr}^{-1}$, respectively. The hourly emissions of the power-plants from reported
420 2015 annual values are 0.74 tonnes $\text{NO}_x \text{ hr}^{-1}$ and 2.56 tonnes $\text{SO}_2 \text{ hr}^{-1}$ (United States EPA, 2018). Our hourly
421 estimates are only preliminary since only half of the plume (approximately) was captured by the measurement
422 transect.

423 The NO_x emission estimates from Sarnia from Day 1 are consistent within 25% and are consistent with the Day 2
424 estimates within the calculated error of approximately $\pm 45\%$ (Fig. 8, Table 4). Some variability between the
425 emission estimates is expected due to wind-data uncertainties, NO_x/NO_2 vertical profile variability, errors introduced
426 by using a constant $\text{VCD}_{\text{influx}}$ and NO_x lifetime, and temporal variations in emissions from the source.

427 Conversion of the hourly measured emissions to annual emissions would require knowledge and application of
428 daily, weekly and seasonal emission profiles, which is beyond the scope of this work. The Mobile-MAX-DOAS
429 emission estimates are reported in units of tonnes per hour since routes were completed within <40 minutes. Events
430 such as flaring can significantly increase the instantaneous emission rate but are excluded from the annual emission
431 inventory data. However, there was no reported flaring during the measurement period (MOECC 2017; personal
432 communication). NO_x emissions from petrochemical facilities, excluding flaring, typically have low variability
433 during periods of continuous operation. According to Ryerson et al. (2003), variation in average hourly NO_x
434 emissions from a petrochemical facility reported by industry (CEMS data) was <10% from an average of the hourly
435 average emissions over 11 days in Houston, Texas. However, this trend may be different for the chemical industry.
436 A first-order comparison to the 2017 National Pollution Release Inventory (NPRI) values (downscaled by assuming
437 constant emissions) was made to determine whether our measured Sarnia emissions are reasonable. The NPRI value
438 is the sum of the NO_x emissions from the top 9 industrial emitters of NO_x in Sarnia whose emissions would have
439 been captured along the driving routes. The NPRI requires significant point source industry facilities to report their
440 pollutant emissions, but the method of estimating emissions can vary by facility (ECCC, 2015). The NPRI emission
441 value does not include mobile and area sources from the Sarnia region. Thus, the NPRI emission inventory values
442 for Sarnia would be expected to be smaller than our measured emissions because of this exclusion. The measured
443 NO_x emissions are larger than the 2017 NPRI value but not statistically so (Fig. 8; Table 4). The exception is the
444 Day 1 route 1* value, which is statistically higher. The average of the four NO_x emission estimates from Sarnia is
445 greater than the 2017 NPRI value. These results demonstrate that our measured emission rates are reasonable. Future

446 Mobile-MAX-DOAS studies could focus on determining diurnal trends in emissions by driving multiple routes at as
447 many times of the day as possible on multiple days, seasons and weekdays/weekends. Measurements of vertical
448 wind profiles could reduce emission uncertainty to allow identification of temporal trends by comparing same-day
449 measurements.

450 Apart from NO_x, we were also able to estimate SO₂ emissions from the Sarnia urban/industrial region during one
451 route when the SO₂ DSCDs were detectable, Day 1 route 3 (Table 5). Our SO₂ emission estimate using the 10 m
452 wind-speed is consistent within error with the 2017 NPRI value (Table 5). We expect our SO₂ emission estimate to
453 be closer to the NPRI values compared to the NO_x estimates because SO₂ emissions from area and mobile sources in
454 Sarnia are expected to be small relative to industrial sources (Ministry of the Environment and Climate Change,
455 2016). Since ships were not operating in the St. Clair River at this time of year, shipping emissions of SO₂ were
456 absent. Thus SO₂ plumes in this region are localized to the major industrial emissions sources. Therefore, the VCDs
457 from the areas unaffected by the Sarnia plumes are representative of background values, VCD_{influx}. While the
458 Mobile-MAX-DOAS was able to capture these plumes (Fig. 9), only 1 of 7 local monitoring stations (LaSalle Road,
459 Fig. S1) observed elevated levels of SO₂ during this period. The under-sampling by stations is due to the highly
460 localized nature of the SO₂ plumes that are from stacks where the plume is frequently elevated above the surface.
461 These results illustrate the complementary nature of Mobile-MAX-DOAS and in-situ measurements and the
462 importance of monitoring techniques that can capture localized plumes independent of the wind direction.

463 3.4.2 Emission Estimates of NOVA Chemicals Industrial Facility

464 NO_x emissions were opportunistically measured from a single facility on Day 3 because the southerly wind-
465 directions isolated this plume (Environment and Climate Change Canada, 2018b) from other industrial sources in
466 Sarnia. The plume originated from Nova Chemicals, the 2nd highest emitter of NO_x in the region in 2017. These
467 conditions allowed us to test the mobile-MAX-DOAS method in isolating a single plume. The wind-direction on
468 Day 3 indicated that the air-masses originated from rural areas south of Sarnia and the VCD_{influx} was expected to be
469 low, $\sim 1 \times 10^{15}$ molec cm⁻².

470 The emission estimates of NO_x from the two routes on Day 3 from the NOVA Chemicals industrial site (Tables 4 &
471 5) are consistent with each other within 10%. The consistency increases confidence in fitting the spectra in each

472 transect against a local FRS and removing influx using the average “background” VCDs rather than using the
473 “DSCD_{Offset}” method in this case. The use of “background” VCDs is appropriate because vehicular traffic upwind of
474 the measurement transect is minimal in the local area. Upwind emissions were unlikely to have contributed
475 significantly to the total measured emissions. The emission estimates from NOVA Chemicals are larger than the
476 2017 NPRI value (Tables 4 & 5). This comparison merely indicates that the Mobile-MAX-DOAS values are
477 reasonable given that there was likely diurnal variability and the measurements were taken only during a single hour
478 on a single day.

479 **3.5 Comparison of OMI Satellite and MAX-DOAS VCDs**

480 The satellite and MAX-DOAS NO₂ VCDs on Day 1 exhibit similar spatial trends in the simple sense that NO₂
481 VCDs increase towards the south from the background regions north of Sarnia (Fig. 10). This trend is probably due
482 to a combination of emissions from U.S.A. power-plants, the Detroit area as well as Sarnia. The NO₂ VCD of the
483 pixel containing the majority of the Sarnia industrial facilities is comparable to rural area VCDs to the north-west of
484 Sarnia. Only 1/8th of the “Sarnia” pixel’s footprint region is likely to be impacted by Sarnia emissions, and the
485 remainder observes mostly rural to semi-rural regions. The OMI Pixel from Day 3 (Fig. 11) containing Sarnia
486 exhibits a minimal increase in NO₂ VCD ($1-2 \times 10^{15}$ molec cm⁻²) compared to the surrounding background regions
487 (Fig. 11). In contrast, the Mobile-MAX-DOAS measurements observed VCD enhancements of up to 1×10^{16} molec
488 cm⁻² within this pixel. The averaging due by the large pixel size (24 km×84 km) causes underestimation of the
489 maximum VCDs. Identification of Sarnia-only emissions without error due to horizontal averaging or inclusion of
490 other sources may require satellite measurements with nadir-viewing pixels centered on Sarnia and/or extremely
491 large averaging times.

492 **3.6 Uncertainties in this Study and Recommended Improvements for Mobile-MAX-DOAS Measurements**

493 Many of the factors that increased the uncertainty in the emission values in this study can be significantly reduced in
494 future through relatively small changes in the method. The many factors have been addressed in Supplemental
495 Information (section S7) and summarized in Table S9. Ideally accurate horizontal flux measurements would require
496 knowledge of the vertical and horizontal profile of pollutant concentrations as well as the vertical and horizontal
497 profile of wind vectors. Lack of knowledge of the vertical profile of wind-speed increases uncertainty in Mobile-

498 MAX-DOAS emission estimates since elevated plumes and well-mixed plumes are transported by winds with
499 typically higher speeds than those near the surface. Future studies could focus on reducing uncertainty by using
500 measurements from sodar, lidar, tall towers, balloon soundings, or a radio acoustic meteorological profiler. In this
501 study, uncertainty was increased (18-30% based on sensitivity analysis; see supplementary S5 & S7) because
502 driving routes could not always include measurements along influx regions (Day 1) due to road proximity to sources
503 or obstructions to the viewing field. Future experiments could measure influx values while stationary at multiple
504 locations along the upwind region chosen for an unobstructed viewing field. Very low background trace-gas levels
505 also resulted in SO₂ DSCDs that were below detection limit most of the time, while being occasionally below
506 detection limit for NO₂ (Fig. 2e). A spectrometer with higher sensitivity giving lower detection limits could solve
507 this issue. Increased averaging of spectra would also improve detectability but at the expense of worse spatial
508 resolution, unless measurements can be made at a slower driving speed. Uncertainty in the NO_x lifetime was a small
509 contribution to uncertainty in this study (up to ±12%) because the distances and transport times between source and
510 measurement locations were relatively small (<25 km). The exception was Day 1 route 1 where uncertainty was up
511 to 30% due to low wind-speeds. The error contribution of NO_x lifetime could be non-trivial if driving routes are far
512 from the sources (e.g., large cities). This error could also be non-trivial if the lifetime that one assumes does not
513 account for the multiple factors discussed in Section 3.3. Bias in the emission estimates from an incorrect lifetime
514 could be avoided by determining NO_x lifetimes from photochemical modelling or, for large cities, satellite
515 observations (Beirle et al., 2011) but taking into account wind speeds (Valin et al., 2013).

516 **4 Conclusions**

517 In this study, we combined Mobile-MAX-DOAS techniques with mobile NO_x measurements and a modular
518 meteorological station to measure emissions of NO_x and SO₂ from the Sarnia region, a relatively small
519 urban/industrial city. Trace-gas VCDs were determined using the DSCD_{offset} method (Wagner et al., 2010) or by
520 fitting measured spectra against a route-local low pollution spectrum. Both methods provided good results, which
521 suggest that the first method is ideal if there are many hours of measurements while the second method is ideal when
522 short routes contain low-pollution regions. Average lower limit Mobile-MAX-DOAS emissions of NO_x from Sarnia
523 were measured to be 1.60 ± 0.34 tonnes hr⁻¹ using 10 m elevation measured wind-speeds. The estimates were larger
524 than the downscaled 2017 NPRI reported industrial emissions of 0.9 tonnes hr⁻¹ (Environment and Climate Change
525 Canada, 2018b) but the NPRI estimate excludes area and mobile emissions. Our lower limit SO₂ emission

526 measurement for Sarnia was 1.81 ± 0.83 tonnes hr^{-1} using 10 m wind-speeds, which is equal within uncertainty to
527 the 2017 NPRI value of 1.85 tonnes hr^{-1} (Environment and Climate Change Canada, 2018c). Our average lower
528 limit NO_x emission measurement from the NOVA Chemicals Facility was 0.28 ± 0.06 tonnes hr^{-1} , the same order of
529 magnitude as the 2016 NPRI value of 0.14 tonnes hr^{-1} (Environment and Climate Change Canada, 2018a).

530 Simultaneous measurements of NO - NO_2 - NO_x improved the accuracy of NO_x emission estimates when plumes of
531 varying ages were observed. The NO_x results from Days 1 and 2 suggest that accurate Mobile-MAX-DOAS NO_x
532 emission measurements from routes that observe plumes with differing ages require accurate knowledge of the
533 localized NO_x/NO_2 ratio.

534 The variability in the ratio of the NO_2 VCDs and mixing ratios indicates that surface NO_2 mixing ratios cannot be
535 reliably estimated from NO_2 VCDs and boundary layer height alone when pollution is emitted from sources of
536 varying heights and chemical composition. A NO_x -analyzer can be an essential component of Mobile-MAX-DOAS
537 NO_2 measurements. The addition of this instrument allows the method to characterize the boundary layer fully and
538 accurately estimate NO_x emissions from NO_2 measurements when multiple NO_x sources are present and when
539 transects are sufficiently distant from the sources.

540 The modular meteorological station improved knowledge of local wind essential to identify time periods of low
541 temporal variability, ensuring low error due to wind estimation. These time periods would have been difficult to
542 identify with only hourly average or modelled wind data. Accurate knowledge of the vertical wind profile would
543 significantly enhance the accuracy of the Mobile-MAX-DOAS emission estimates. Future studies could obtain
544 vertical wind profiles using sodar, lidar, wind-rass, and radiosonde on a weather balloon or local aircraft soundings.

545 Mobile-MAX-DOAS measurements identified significant OMI intrapixel inhomogeneity and observed industrial
546 pollution enhancements that were poorly captured by the in-situ ground stations. These results suggest that Mobile-
547 MAX-DOAS has clear advantages in similar industrial regions over other remote sensing techniques used for
548 estimating emissions (e.g., using aircraft or satellite): higher spatial resolution, the potential for multiple emission
549 estimates per day (i.e., observations of diurnal trends), and much lower operational costs. Mobile-MAX-DOAS is a
550 “top-down” low-cost solution for validating bottom-up inventories that compliments in-situ monitoring and has

551 significant utility in smaller regions with significant emissions where satellite applications are limited. Future
552 Mobile-MAX-DOAS studies in such regions can focus on measuring temporal trends in emissions.

553 **Author Contributions**

554 ZD conceived of and organized the field campaign with aid from RM. ZD, SB, AK, WF, CC and RM carried out the
555 experiments in Sarnia. CM modelled conditions for the satellite retrievals of NO₂ in the region of Sarnia and
556 provided useful advice. ZD and RM prepared the manuscript, with contributions from all co-authors.

557 **Acknowledgements**

558 This study was completed with collaborative support by the Ontario Ministry of the Environment and Climate
559 Change. Funding for the study was provided by NSERC, CREATE IACPES and the York University Faculty of
560 Graduate Studies. The corresponding author would like to thank Mr. Barry Duffey at the Ontario Ministry of
561 Environment and Climate Change for his support at the project start. We also thank Tony Munoz of OME for his
562 continued support of our research.

563 **References**

- 564 Alicke, B., Platt, U., and Stutz, J.: Impact of nitrous acid photolysis on the total hydroxyl radical budget during the
565 limitation of oxidant production/Pianura Padana Produzione di Ozono study in Milan, *J. Geophys. Res.*, 107(D22),
566 8196, doi:10.1029/2000JD000075, 2002.
- 567 Baray, S., Darlington, A., Gordon, M., Hayden, K. L., Leithead, A., Li, S.-M., Liu, P. S. K., Mittermeier, R. L.,
568 Moussa, S. G., O'Brien, J., Staebler, R., Wolde, M., Worthy, D. and McLaren, R.: Quantification of methane
569 sources in the Athabasca Oil Sands Region of Alberta by aircraft mass balance, *Atmospheric Chem. Phys.*, 18(10),
570 7361–7378, doi:10.5194/acp-18-7361-2018, 2018.
- 571 Beirle, S., Boersma, K. F., Platt, U., Lawrence, M. G. and Wagner, T.: Megacity Emissions and Lifetimes of
572 Nitrogen Oxides Probed from Space, *Science*, 333(6050), 1737–1739, doi:10.1126/science.1207824, 2011.
- 573 Boersma, K. F., Eskes, H. J., Veefkind, J. P., Brinksma, E. J., Van der A, R. J., Sneep, M., van den Oord, G. H. J.,
574 Levelt, P. F., Stammes, P., Gleason, J. F. and Bucsela, E. J.: Near-real time retrieval of tropospheric NO₂ from OMI,
575 *Atmospheric Chem. Phys.*, 7(8), 2103–2118, 2007.
- 576 Bogumil, K., Orphal, J., Homann, T., Voigt, S., Spietz, P., Fleischmann, O. C., Vogel, A., Hartmann, M.,
577 Kromminga, H., Bovensmann, H., Frerick, J. and Burrows, J. P.: Measurements of molecular absorption spectra
578 with the SCIAMACHY pre-flight model: instrument characterization and reference data for atmospheric remote-
579 sensing in the 230–2380 nm region, *J. Photochem. Photobiol. Chem.*, 157(2–3), 167–184, doi:10.1016/S1010-
580 6030(03)00062-5, 2003.
- 581 Brinksma, E. J., Pinardi, G., Volten, H., Braak, R., Richter, A., Schoenhardt, A., van Roozendaal, M., Fayt, C.,
582 Hermans, C., Dirksen, R. J., Vlemmix, T., Berkhout, A. J. C., Swart, D. P. J., Oetjen, H., Wittrock, F., Wagner, T.,
583 Ibrahim, O. W., de Leeuw, G., Moerman, M., Curier, R. L., Celarier, E. A., Cede, A., Knap, W. H., Veefkind, J. P.,
584 Eskes, H. J., Allaart, M., Rothe, R., Peters, A. J. M. and Levelt, P. F.: The 2005 and 2006 DANDELIONS NO₂ and

585 aerosol intercomparison campaigns, *J. Geophys. Res.-Atmospheres*, 113(D16), D16S46,
586 doi:10.1029/2007JD008808, 2008.

587 Brown, S. S., Dube, W. P., Karamchandani, P., Yarwood, G., Peischl, J., Ryerson, T. B., Neuman, J. A., Nowak, J.
588 B., Holloway, J. S., Washenfelder, R. A., Brock, C. A., Frost, G. J., Trainer, M., Parrish, D. D., Fehsenfeld, F. C.
589 and Ravishankara, A. R.: Effects of NO_x control and plume mixing on nighttime chemical processing of plumes
590 from coal-fired power plants, *J. Geophys. Res.-Atmospheres*, 117, D07304, doi:10.1029/2011JD016954, 2012.

591 Davis, Z. Y. W., Frieß, U., Strawbridge, K. B., Aggarwal, M., Baray, S., Schnitzler, E. G., Lobo, A., Fioletov, V.
592 E., Abboud, I., McLinden, C. A., Whiteway, J., Willis, M. D., Lee, A. K. Y., Brook, J., Olfert, J., O'Brien, J.,
593 Staebler, R., Osthoff, H. D., Mihele, C., and McLaren, R.: Validation of MAX-DOAS retrievals of aerosol
594 extinction, SO₂ and NO₂ through comparison with lidar, sun photometer, Active-DOAS and aircraft measurements
595 in the Athabasca Oil Sands Region, *Atmos. Meas. Tech. Discuss.*, <https://doi.org/10.5194/amt-2019-296>, in review,
596 2019.

597 Dragomir, C. M., Constantin, D.-E., Voiculescu, M., Georgescu, L. P., Merlaud, A. and Van Roozendaal, M.:
598 Modeling results of atmospheric dispersion of NO₂ in an urban area using METI-LIS and comparison with
599 coincident mobile DOAS measurements, *Atmos. Pollut. Res.*, 6(3), 503–510, doi:10.5094/APR.2015.056, 2015.

600 Dunlea, E. J., Herndon, S. C., Nelson, D. D., Volkamer, R. M., San Martini, F., Sheehy, P. M., Zahniser, M. S.,
601 Shorter, J. H., Wormhoudt, J. C., Lamb, B. K., Allwine, E. J., Gaffney, J. S., Marley, N. A., Grutter, M., Marquez,
602 C., Blanco, S., Cardenas, B., Retama, A., Ramos Villegas, C. R., Kolb, C. E., Molina, L. T., and Molina, M. J.:
603 Evaluation of nitrogen dioxide chemiluminescence monitors in a polluted urban environment, *Atmos. Chem. Phys.*,
604 7, 2691-2704, 10.5194/acp-7-2691-2007, 2007.

605 Environment and Climate Change Canada.: Using and interpreting data from the National Pollutant Release
606 Inventory, aem [online] Available from: [https://www.canada.ca/en/environment-climate-change/services/national-](https://www.canada.ca/en/environment-climate-change/services/national-pollutant-release-inventory/using-interpreting-data.html)
607 [pollutant-release-inventory/using-interpreting-data.html](https://www.canada.ca/en/environment-climate-change/services/national-pollutant-release-inventory/using-interpreting-data.html) (Accessed 1 August 2018), 2015.

608 Environment and Climate Change Canada: NPRI Data Search - Facility and Substance Information - NOVA
609 Chemicals (Canada) Ltd. - Corunna Site 2017, [online] Available from: [https://pollution-waste.canada.ca/national-](https://pollution-waste.canada.ca/national-release-inventory/archives/index.cfm)
610 [release-inventory/archives/index.cfm](https://pollution-waste.canada.ca/national-release-inventory/archives/index.cfm) (Accessed 17 September 2018a), 2018.

611 Environment and Climate Change Canada: NPRI Data Search - Facility Search Results Nitrogen oxides (expressed
612 as NO₂) (11104-93-1), [online] Available from: [https://pollution-waste.canada.ca/national-release-](https://pollution-waste.canada.ca/national-release-inventory/archives/index.cfm)
613 [inventory/archives/index.cfm](https://pollution-waste.canada.ca/national-release-inventory/archives/index.cfm) (Accessed 17 September 2018b), 2018.

614 Environment and Climate Change Canada: NPRI Data Search - Facility Search Results Sulphur Dioxide (7446-09-
615 5), [online] Available from: <https://pollution-waste.canada.ca/national-release-inventory/archives/index.cfm>
616 (Accessed 17 September 2018c), 2018.

617 Environment and Climate Change Canada: NPRI Facility Search Results - Volatile Organic Compounds (VOCs)
618 (NA-M16), [online] Available from: <https://pollution-waste.canada.ca/national-release-inventory/archives/index.cfm>
619 (Accessed 17 September 2018d), 2018.

620 Finlayson-Pitts, B. J. and Pitts, J.N.: *Chemistry of the Upper and Lower Atmosphere*, Academic Press, San Diego
621 CA, 969 pp., 2000.

622 Friess, U., Monks, P. S., Remedios, J. J., Rozanov, A., Sinreich, R., Wagner, T. and Platt, U.: MAX-DOAS O₄
623 measurements: A new technique to derive information on atmospheric aerosols: 2. Modeling studies, *J. Geophys.*
624 *Res.-Atmospheres*, 111(D14), D14203, doi:10.1029/2005JD006618, 2006.

- 625 Gordon, M., Li, S.-M., Staebler, R., Darlington, A., Hayden, K., O'Brien, J. and Wolde, M.: Determining air
626 pollutant emission rates based on mass balance using airborne measurement data over the Alberta oil sands
627 operations, *Atmos. Meas. Tech.*, 8(9), 3745–3765, doi:10.5194/amt-8-3745-2015, 2015.
- 628 Halla, J. D., Wagner, T., Beirle, S., Brook, J. R., Hayden, K. L., O'Brien, J. M., Ng, A., Majonis, D., Wenig, M. O.
629 and McLaren, R.: Determination of tropospheric vertical columns of NO₂ and aerosol optical properties in a rural
630 setting using MAX-DOAS, *Atmos. Chem. Phys.*, 11(23), 12475–12498, doi:10.5194/acp-11-12475-2011, 2011.
- 631 Heckel, A., Richter, A., Tarsu, T., Wittrock, F., Hak, C., Pundt, I., Junkermann, W. and Burrows, J. P.: MAX-DOAS
632 measurements of formaldehyde in the Po-Valley, *Atmos. Chem. Phys.*, 5, 909–918, doi:10.5194/acp-5-909-2005,
633 2005.
- 634 Heckel, A., Kim, S.-W., Frost, G. J., Richter, A., Trainer, M. and Burrows, J. P.: Influence of low spatial resolution
635 a priori data on tropospheric NO₂ satellite retrievals, *Atmos. Meas. Tech.*, 4(9), 1805–1820, doi:10.5194/amt-4-
636 1805-2011, 2011.
- 637 Honninger, G. and Platt, U.: Observations of BrO and its vertical distribution during surface ozone depletion at
638 Alert, *Atmos. Environ.*, 36(15–16), 2481–2489, doi:10.1016/S1352-2310(02)00104-8, 2002.
- 639 Honninger, G., von Friedeburg, C. and Platt, U.: Multi axis differential optical absorption spectroscopy (MAX-
640 DOAS), *Atmos. Chem. Phys.*, 4, 231–254, 2004.
- 641 Huang, M., Bowman, K. W., Carmichael, G. R., Chai, T., Pierce, R. B., Worden, J. R., Luo, M., Pollack, I. B.,
642 Ryerson, T. B., Nowak, J. B., Neuman, J. A., Roberts, J. M., Atlas, E. L. and Blake, D. R.: Changes in nitrogen
643 oxides emissions in California during 2005–2010 indicated from top-down and bottom-up emission estimates, *J.*
644 *Geophys. Res.-Atmospheres*, 119(22), 12928–12952, doi:10.1002/2014JD022268, 2014.
- 645 Ialongo, I., Hakkarainen, J., Hyttinen, N., Jalkanen, J.-P., Johansson, L., Boersma, K. F., Krotkov, N. and
646 Tamminen, J.: Characterization of OMI tropospheric NO₂ over the Baltic Sea region, *Atmos. Chem. Phys.*, 14(15),
647 7795–7805, doi:10.5194/acp-14-7795-2014, 2014.
- 648 Ialongo, I., Herman, J., Krotkov, N., Lamsal, L., Boersma, K. F., Hovila, J. and Tamminen, J.: Comparison of OMI
649 NO₂ observations and their seasonal and weekly cycles with ground-based measurements in Helsinki, *Atmos. Meas.*
650 *Tech.*, 9(10), 5203–5212, doi:10.5194/amt-9-5203-2016, 2016.
- 651 Ibrahim, O., Shaiganfar, R., Sinreich, R., Stein, T., Platt, U. and Wagner, T.: Car MAX-DOAS measurements
652 around entire cities: quantification of NO_x emissions from the cities of Mannheim and Ludwigshafen (Germany),
653 *Atmos. Meas. Tech.*, 3(3), 709–721, doi:10.5194/amt-3-709-2010, 2010.
- 654 Irie, H., Kanaya, Y., Akimoto, H., Iwabuchi, H., Shimizu, A. and Aoki, K.: First retrieval of tropospheric aerosol
655 profiles using MAX-DOAS and comparison with lidar and sky radiometer measurements, *Atmos. Chem. Phys.*,
656 8(2), 341–350, doi:10.5194/acp-8-341-2008, 2008.
- 657 Kim, N. K., Kim, Y. P., Morino, Y., Kurokawa, J. and Ohara, T.: Verification of NO_x emission inventories over
658 North Korea, *Environ. Pollut.*, 195, 236–244, doi:10.1016/j.envpol.2014.06.034, 2014.
- 659 Leighton, P. A.: *Photochemistry of air pollution*. --, Academic Press, New York., 1961.
- 660 Liu, F., Beirle, S., Zhang, Q., Doerner, S., He, K. and Wagner, T.: NO_x lifetimes and emissions of cities and power
661 plants in polluted background estimated by satellite observations, *Atmos. Chem. Phys.*, 16(8), 5283–5298,
662 doi:10.5194/acp-16-5283-2016, 2016.
- 663 McLinden, C. A., Fioletov, V., Boersma, K. F., Krotkov, N., Sioris, C. E., Veefkind, J. P. and Yang, K.: Air quality
664 over the Canadian oil sands: A first assessment using satellite observations, *Geophys. Res. Lett.*, 39, L04804,
665 doi:10.1029/2011GL050273, 2012.

- 666 Ministry of the Environment and Climate Change: Air Quality in Ontario 2014 Report, 2015. [online] Available
667 from: <https://www.ontario.ca/page/air-quality-ontario-2014-report> (Accessed 17 Sept. 2019).
- 668 Ministry of the Environment and Climate Change: Air Quality in Ontario 2016 Report., 2017. [online] Available
669 from: <https://www.ontario.ca/document/air-quality-ontario-2016-report> (Accessed 17 Sept. 2019).
- 670 Nunnermacker, L. J., Kleinman, L. I., Imre, D., Daum, P. H., Lee, Y.-N., Lee, J. H., Springston, S. R., Newman, L.
671 and Gillani, N.: NO_y lifetimes and O₃ production efficiencies in urban and power plant plumes: Analysis of field
672 data, *J. Geophys. Res. Atmospheres*, 105(D7), 9165–9176, doi:10.1029/1999JD900753, 2000.
- 673 Oiamo, T. H., Luginaah, I. N., Atari, D. O. and Gorey, K. M.: Air pollution and general practitioner access and
674 utilization: a population based study in Sarnia, 'Chemical Valley,' Ontario, *Environ. Health*, 10, doi:10.1186/1476-
675 069X-10-71, 2011.
- 676 Platt, U., Perner, D. and Patz, H.: Simultaneous Measurement of Atmospheric CH₂O, O₃, and NO₂ by Differential
677 Optical-Absorption, *J. Geophys. Res.-Oceans Atmospheres*, 84(NC10), 6329–6335, doi:10.1029/JC084iC10p06329,
678 1979.
- 679 Platt, U., Perner, D., Harris, G.W., Winer, A. M., and Pitts Jr., J. N.: Observations of nitrous acid in an urban
680 atmosphere by differential optical absorption, *Nature*, 285, 312–314, 1980.
- 681 Platt, U., Stutz, J., Springer E-books - York University and SpringerLink (Online service): Differential optical
682 absorption spectroscopy: principles and applications, Springer Verlag, Berlin. [online] Available from:
683 <http://www.library.yorku.ca/eresolver/?id=1261530>, 2008.
- 684 Rivera, C., Mellqvist, J., Samuelsson, J., Lefer, B., Alvarez, S., and Patel, M. R.: Quantification of NO₂ and SO₂
685 emissions from the Houston Ship Channel and Texas City industrial areas during the 2006 Texas Air Quality Study,
686 *Journal of Geophysical Research: Atmospheres*, 115, 10.1029/2009jd012675, 2010.
- 687 Ryerson, T. B., Trainer, M., Angevine, W. M., Brock, C. A., Dissly, R. W., Fehsenfeld, F. C., Frost, G. J., Goldan,
688 P. D., Holloway, J. S., Hubler, G., Jakoubek, R. O., Kuster, W. C., Neuman, J. A., Nicks, D. K., Parrish, D. D.,
689 Roberts, J. M., Sueper, D. T., Atlas, E. L., Donnelly, S. G., Flocke, F., Fried, A., Potter, W. T., Schauffler, S.,
690 Stroud, V., Weinheimer, A. J., Wert, B. P., Wiedinmyer, C., Alvarez, R. J., Banta, R. M., Darby, L. S. and Senff, C.
691 J.: Effect of petrochemical industrial emissions of reactive alkenes and NO_x on tropospheric ozone formation in
692 Houston, Texas, *J. Geophys. Res.-Atmospheres*, 108(D8), 4249, doi:10.1029/2002JD003070, 2003.
- 693 Seinfeld, J. H. and Pandis, S. N.: *Atmospheric Chemistry and Physics: From Air Pollution to Climate Change*, John
694 Wiley & Sons., 2006.
- 695 Shabbir, Y., Khokhar, M. F., Shaiganfar, R. and Wagner, T.: Spatial variance and assessment of nitrogen dioxide
696 pollution in major cities of Pakistan along N5-Highway, *J. Environ. Sci.*, 43(Supplement C), 4–14,
697 doi:10.1016/j.jes.2015.04.038, 2016.
- 698 Shaiganfar, R., Beirle, S., Sharma, M., Chauhan, A., Singh, R. P. and Wagner, T.: Estimation of NO_x emissions
699 from Delhi using Car MAX-DOAS observations and comparison with OMI satellite data, *Atmos. Chem. Phys.*,
700 11(21), 10871–10887, doi:10.5194/acp-11-10871-2011, 2011.
- 701 Shaiganfar, R., Beirle, S., Petetin, H., Zhang, Q., Beekmann, M. and Wagner, T.: New concepts for the comparison
702 of tropospheric NO₂ column densities derived from car-MAX-DOAS observations, OMI satellite observations and
703 the regional model CHIMERE during two MEGAPOLI campaigns in Paris 2009/10, *Atmos. Meas. Tech.*, 8(7),
704 2827–2852, doi:10.5194/amt-8-2827-2015, 2015.
- 705 Shaiganfar, R., Beirle, S., van der Gon, H. D., Jonkers, S., Kuenen, J., Petetin, H., Zhang, Q., Beekmann, M. and
706 Wagner, T.: Estimation of the Paris NO_x emissions from mobile MAX-DOAS observations and CHIMERE model

707 simulations during the MEGAPOLI campaign using the closed integral method, *Atmos. Chem. Phys.*, 17(12), 7853–
708 7890, doi:10.5194/acp-17-7853-2017, 2017.

709 Tokarek, T. W., Odame-Ankrah, C. A., Huo, J. A., McLaren, R., Lee, A. K. Y., Adam, M. G., Willis, M. D., Abbatt,
710 J. P. D., Mihele, C., Darlington, A., Mittermeier, R. L., Strawbridge, K., Hayden, K. L., Olfert, J. S., Schnitzler, E.
711 G., Brownsey, D. K., Assad, F. V., Wentworth, G. R., Tevlin, A. G., Worthy, D. E. J., Li, S.-M., Liggio, J., Brook, J.
712 R. and Osthoff, H. D.: Principal component analysis of summertime ground site measurements in the Athabasca oil
713 sands with a focus on analytically unresolved intermediate volatility organic compounds, *Atmos. Chem. Phys.*,
714 2018, 17819-17841, doi:10.5194/acp-18-17819-2018, 2018.

715 United States EPA: Air Pollutant Report | ECHO | US EPA, Air Pollut. Rep. [online] Available from:
716 <https://echo.epa.gov/air-pollutant-report?fid=110000404740> (Accessed 2 August 2018), 2018.

717 Valin, L. C., Russell, A. R. and Cohen, R. C.: Variations of OH radical in an urban plume inferred from NO₂ column
718 measurements, *Geophys. Res. Lett.*, 40(9), 1856–1860, doi:10.1002/grl.50267, 2013.

719 Wagner, T., Dix, B., von Friedeburg, C., Friess, U., Sanghavi, S., Sinreich, R. and Platt, U.: MAX-DOAS O-4
720 measurements: A new technique to derive information on atmospheric aerosols - Principles and information content,
721 *J. Geophys. Res.-Atmospheres*, 109(D22), D22205, doi:10.1029/2004JD004904, 2004.

722 Wagner, T., Ibrahim, O., Shaiganfar, R. and Platt, U.: Mobile MAX-DOAS observations of tropospheric trace gases,
723 *Atmos. Meas. Tech.*, 3(1), 129–140, 2010.

724 Wagner, T., Beirle, S., Brauers, T., Deutschmann, T., Friess, U., Hak, C., Halla, J. D., Heue, K. P., Junkermann, W.,
725 Li, X., Platt, U. and Pundt-Gruber, I.: Inversion of tropospheric profiles of aerosol extinction and HCHO and NO₂
726 mixing ratios from MAX-DOAS observations in Milano during the summer of 2003 and comparison with
727 independent data sets, *Atmos. Meas. Tech.*, 4(12), 2685–2715, doi:10.5194/amt-4-2685-2011, 2011.

728 Wiegand, A. N. and Bofinger, N. D.: Review of empirical methods for the calculation of the diurnal NO₂ photolysis
729 rate coefficient, *Atmos. Environ.*, 34(1), 99–108, doi:10.1016/S1352-2310(99)00294-0, 2000.

730 Wu, F., Li, A., Xie, P., Chen, H., Hu, Z., Zhang, Q., Liu, J. and Liu, W.: Emission Flux Measurement Error with a
731 Mobile DOAS System and Application to NO_x Flux Observations, *Sensors*, 17(2), doi:10.3390/s17020231, 2017.

732

733 **Table 1** Daily meteorological conditions, number of routes and time period of routes driven. Wind-speed from
 734 SLEA LaSalle Road; Temperature and Relative Humidity from portable meteorological station Day 1 and Day 2 and
 735 from Moore Line station Day 2.

Date	Number of Routes Driven	Measurement Local Time Period	Average Wind-speed (km hr ⁻¹)	Prevailing Wind-Direction	Average Temperature (°C)	Average Relative Humidity (%)	Emission Area Measured
3/21/2017	4	10:26-13:16	15	Westerly	10	50	City of Sarnia
3/22/2017	1	17:22-17:41	8	Northerly	-3	52	City of Sarnia
3/23/2017	2	11:10-11:57	15	Southerly	1	42	NOVA Chemicals Industries Facility

736

737 **Table 2** NO_x/NO₂ ratios for routes driven.

Date	Day's	Measurement	Number of	Average $\pm 1\sigma$	Median
	Route	Local Time			
	Number	Period			
3/21/2017	1	10:26-11:06	37	1.53 \pm 0.12	1.49
3/21/2017	2	11:22-11:45	23	1.45 \pm 0.06	1.44
3/21/2017	3	12:09-12:28	18	1.36 \pm 0.07	1.37
3/21/2017	4	12:34-13:16	24	1.29 \pm 0.06	1.31
3/22/2017	1	17:22-17:41	10	1.49 \pm 0.53	1.30
3/22/2017	1	17:22-17:41*	9	1.32 \pm 0.08	1.30
3/23/2017	1	11:10-11:19	5	1.39 \pm 0.09	1.39
3/23/2017	2	11:42-11:57	9	1.46 \pm 0.17	1.52

738 The 3/22/2017 17:22-17:41* data had the peak NO₂ plume location NO_x/NO₂ value removed.

739

740 **Table 3** Calculated Leighton Ratios for selected plume maximums on Day 1 and 2.

Date	Local Time	J_{NO_2} ($\times 10^{-3} \text{ s}^{-1}$)	Solar Irradiance (W m^{-2})	Solar Zenith Angle	O_3 mixing ratio (ppb)	Measured NO_2/NO (ppb ppb^{-1})	Calculated Leighton Ratio*
21/03/2017	11:00	5.23	564	35	18	1.7	1.61
21/03/2017	11:30	5.65	600	40	23	2.2	1.76
21/03/2017	12:15	6.44	675	43	23	2.2	2.01
22/03/2017	17:28	2.71	300	23	10	0.5	0.44

741 * **Note that Leighton ratios, ϕ** , could be biased high by as much as +20% from the the NO_z component of NO_y measured by the
 742 NO_x analyzer, but likely much lower due to it being a fresh urban/industrial NO_x plume.

743

744 **Table 4** Lower limit NO_x Emission Estimates from 10 m elevation wind-speeds.

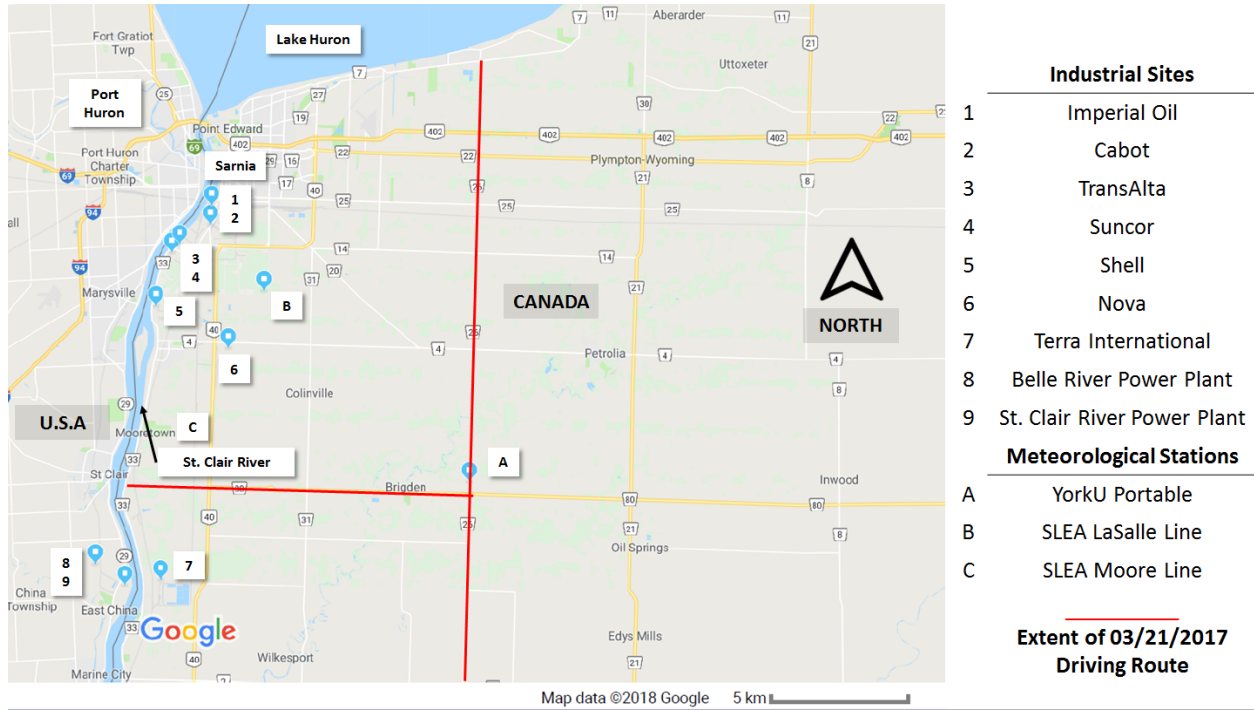
Date	Emission Source	Daily Route Number	Lower-limit NO _x (tonnes hr ⁻¹)	NPRI NO _x (tonnes hr ⁻¹)
21/03/2017	Sarnia	1	1.6±0.8	0.9
21/03/2017	Sarnia	2	1.2±0.5	0.9
21/03/2017	Sarnia	3	1.4±0.5	0.9
22/03/2017	Sarnia	1	1.5±0.6	0.9
22/03/2017	Sarnia	1*	2.2±0.8	0.9
23/03/2017	NovaChem	1	0.27±0.1	0.14
23/03/2017	NovaChem	2	0.29±0.1	0.14

745 * calculated using individual NO_x/NO₂ ratios.

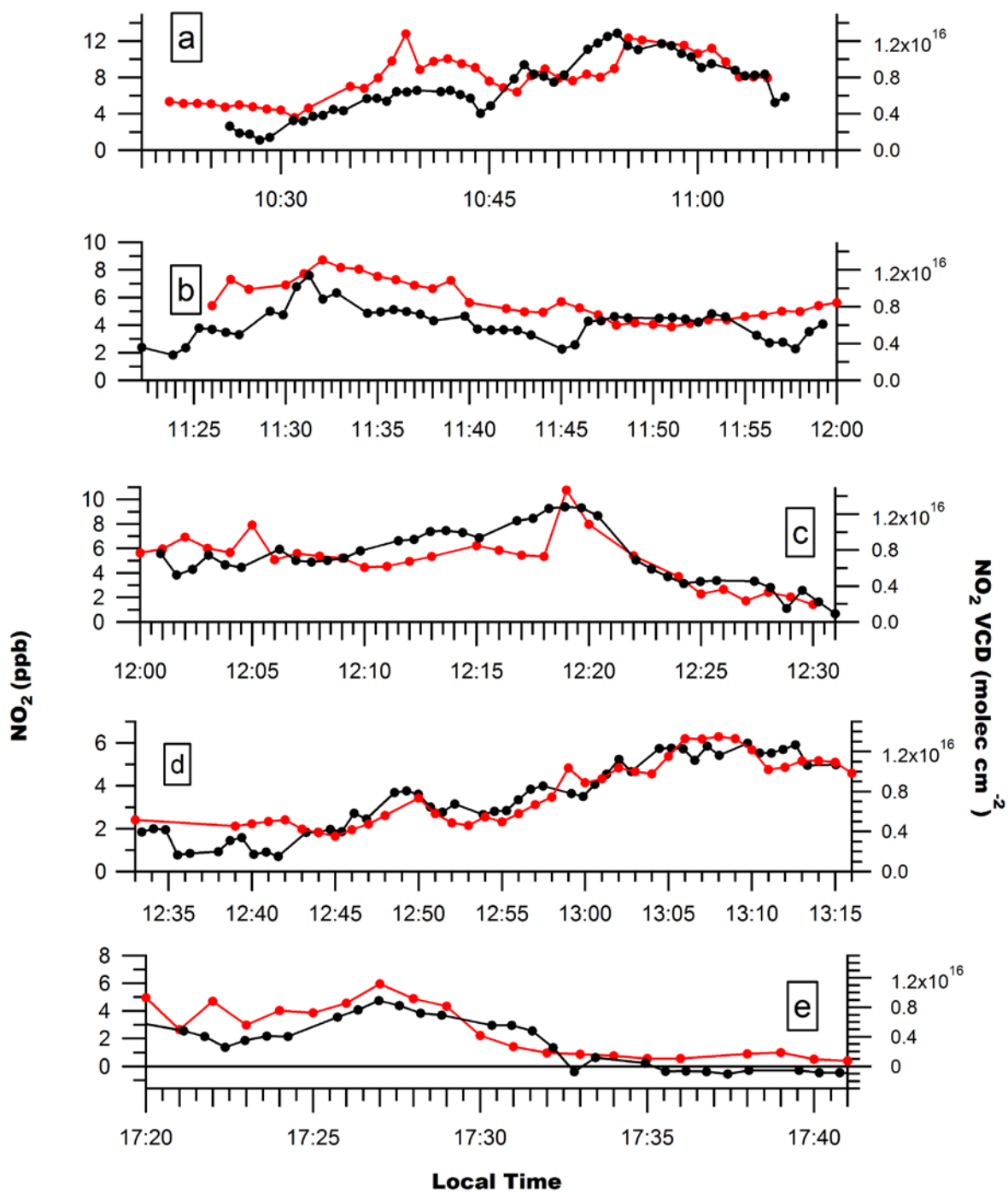
746 **Table 5** Average emission estimates from Mobile MAX_DOAS using 10 m wind-speeds and from NPRI.

	Gas	Lower Limit Emission Estimate (tonnes hr ⁻¹)	2017 NPRI Value (tonnes hr ⁻¹)
Sarnia	NO _x	1.60±0.34	0.9
Sarnia	SO ₂	1.81±0.83	1.85
NOVA Chemicals- Corunna Site	NO _x	0.28±0.06	0.14

747



748 **Figure 1** Location of industrial NO_x and SO₂ emission sources and meteorological stations in the Sarnia area.



749

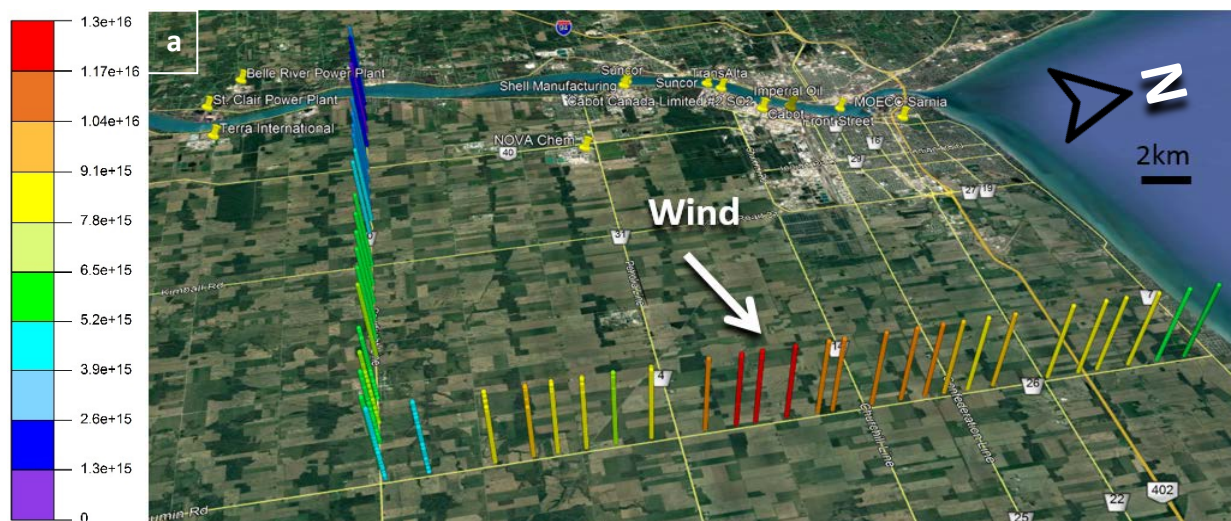
750 **Figure 2** NO₂ mixing ratios and NO₂ VCDs along routes 1-4 on Day 1 (a) – (d) and route 1 on Day 2 (e).

751 Uncertainties in measured NO₂ mixing ratios are ± 0.5 ppb. Uncertainties in the NO₂ VCD are given by

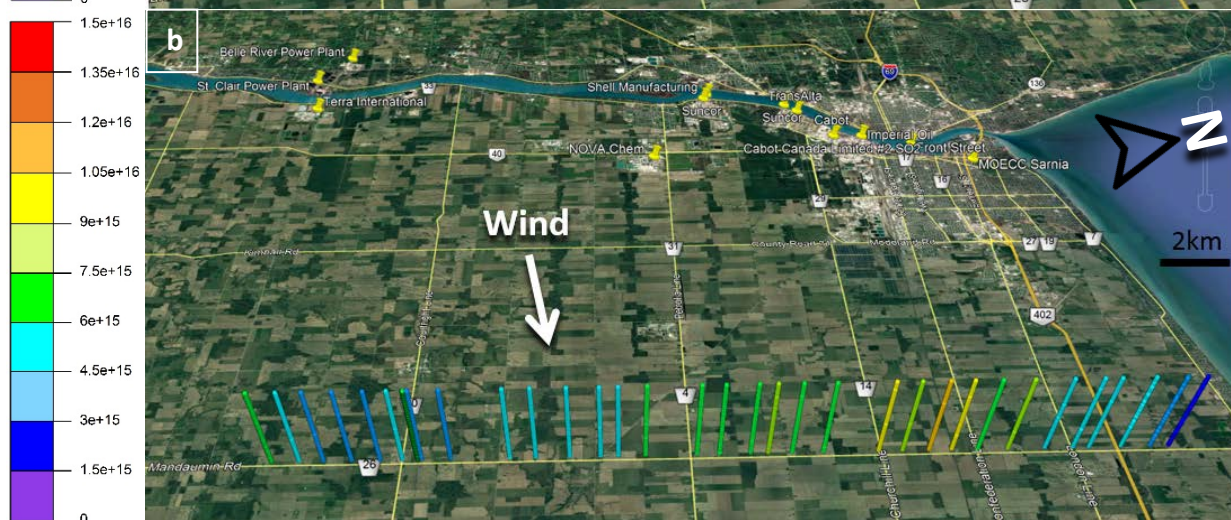
752 $\sigma_{\text{VCD}} = [(0.25 \text{ VCD})^2 + (5 \times 10^{14} \text{ molec cm}^{-2})^2]^{1/2}$.

753

754



755



756

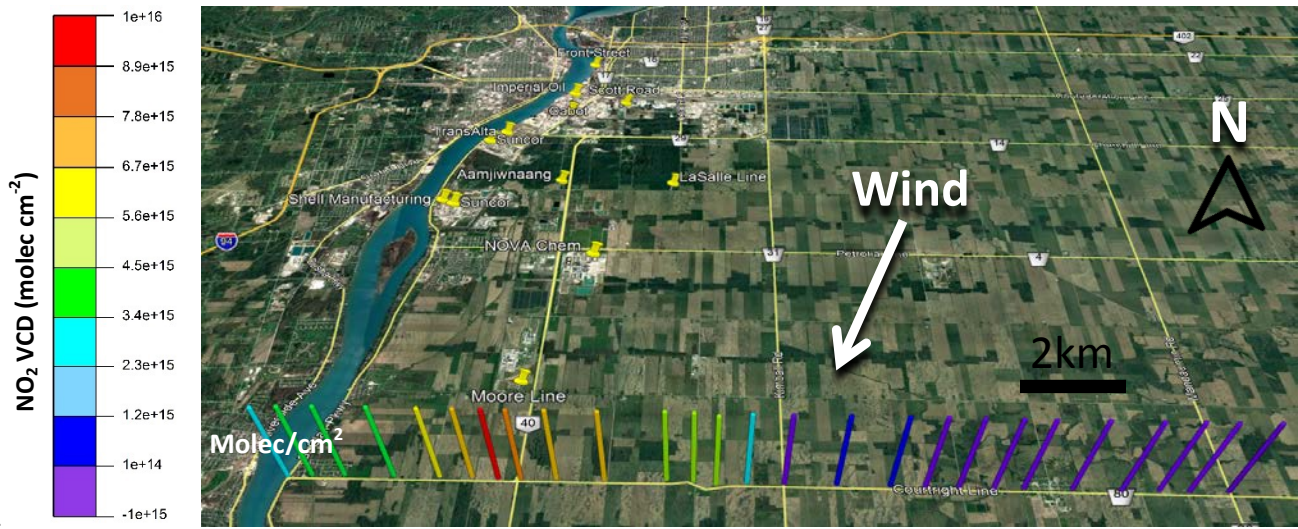


757

758

759 **Figure 3** Day 1 driving routes; (a) route 1, (b) route 2 and (c) route 3, used to estimate NO_x emissions from Sarnia.

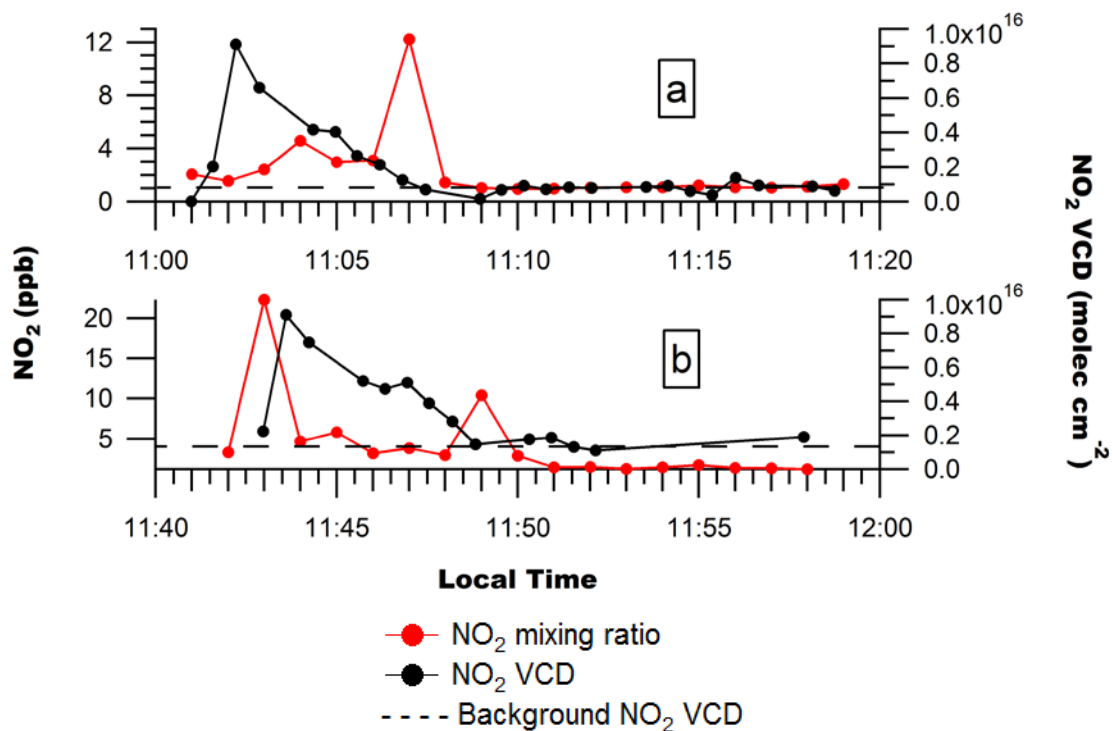
760
761



762
763
764
765

Figure 4 NO₂ VCDs measured on Day 2 route 1.

766



767

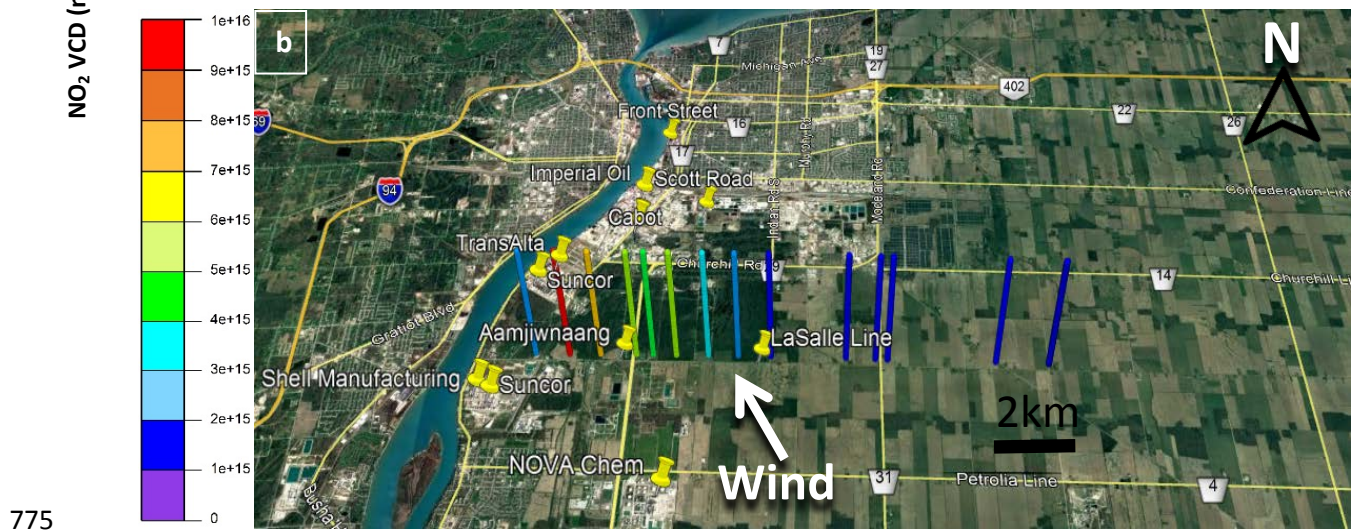
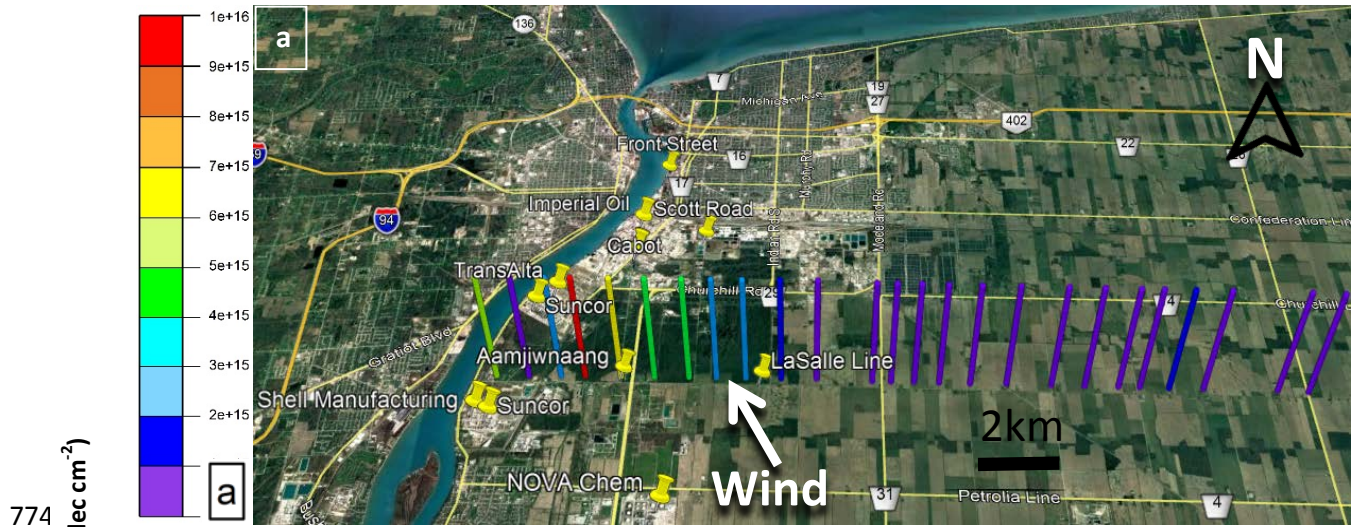
768
769

770 **Figure 5** NO₂ mixing ratios and NO₂ VCDs measured on Day 3 along (a) driving route 1 and (b) driving route 2.

771 Uncertainties in measured NO₂ mixing ratios are ± 0.5 ppb. Uncertainties in the NO₂ VCD are given by

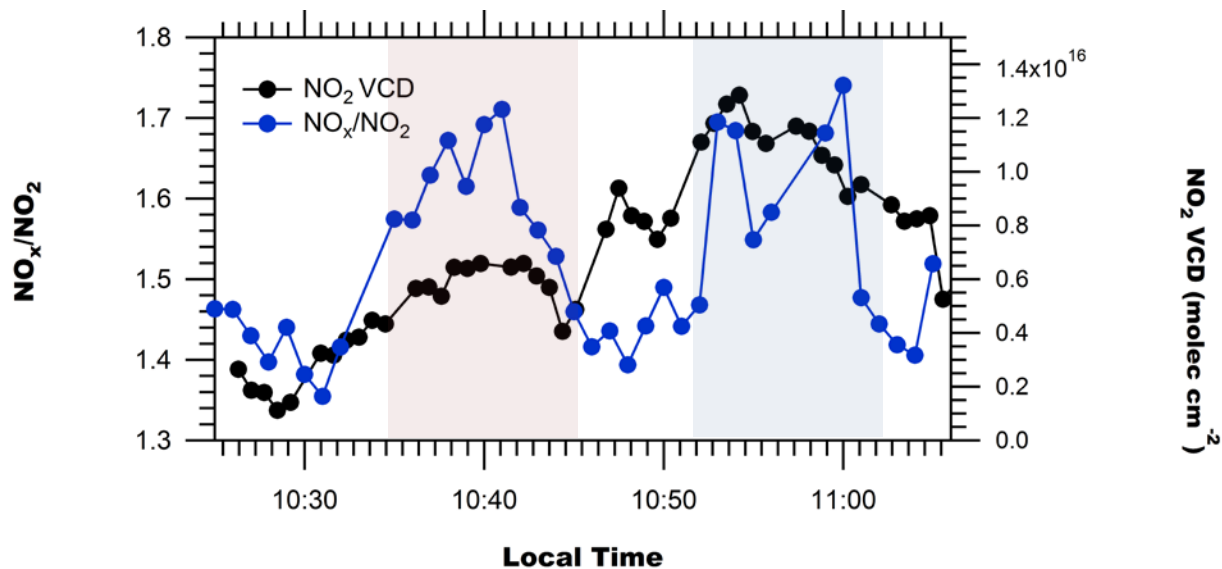
772 $\sigma_{\text{VCD}} = [(0.25 \text{ VCD})^2 + (5 \times 10^{14} \text{ molec cm}^{-2})^2]^{1/2}$.

773



776 **Figure 6** NO₂ VCDs measured on Day 3 along (a) driving route 1 and (b) driving route 2.

777

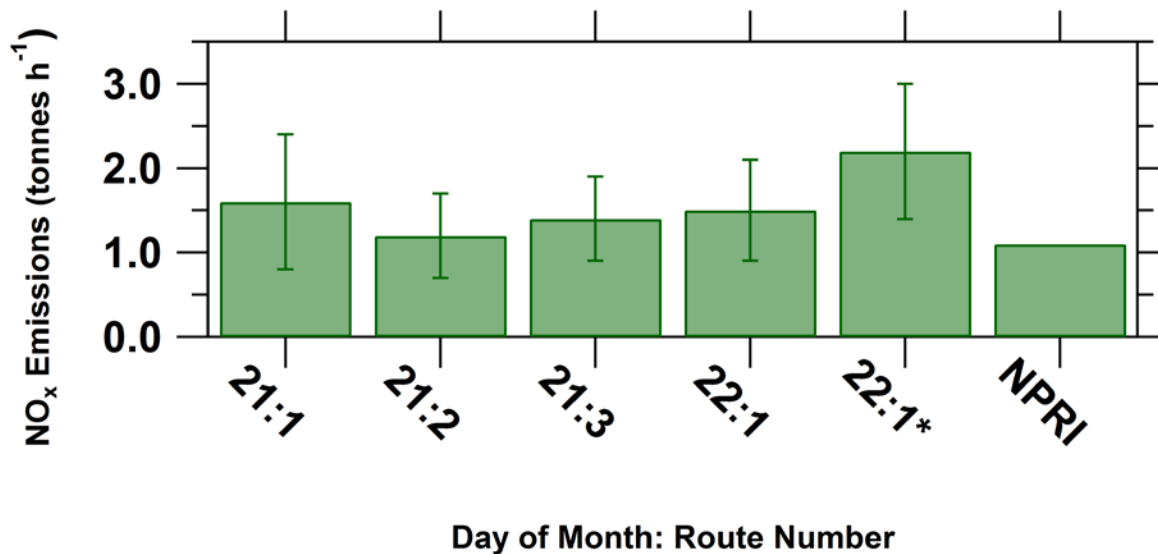


778

779 **Figure 7** NO₂ VCDs and NO_x/NO₂ ratios on Day 1 route 1. Detection of Michigan power plants' plume(s) (left) on
 780 East-West transect & Sarnia plume (right) on North-South transect are highlighted in pink and blue,
 781 respectively. Uncertainties in measured NO_x/NO₂ ratios are ± 5% (~±0.075). Uncertainties in the NO₂
 782 VCD are given by $\sigma_{\text{VCD}} = [(0.25 \text{ VCD})^2 + (5 \times 10^{14} \text{ molec cm}^{-2})^2]^{1/2}$.

783

784



785

786 **Figure 8** Lower limit estimates of NO_x Emissions from Sarnia on Day 1 and Day 3 and 2016 NPRI emissions. The
 787 22:1* NO_x emission estimate used individual NO_x/NO₂ ratio values for each VCDs rather than a single average
 788 ratio.

789

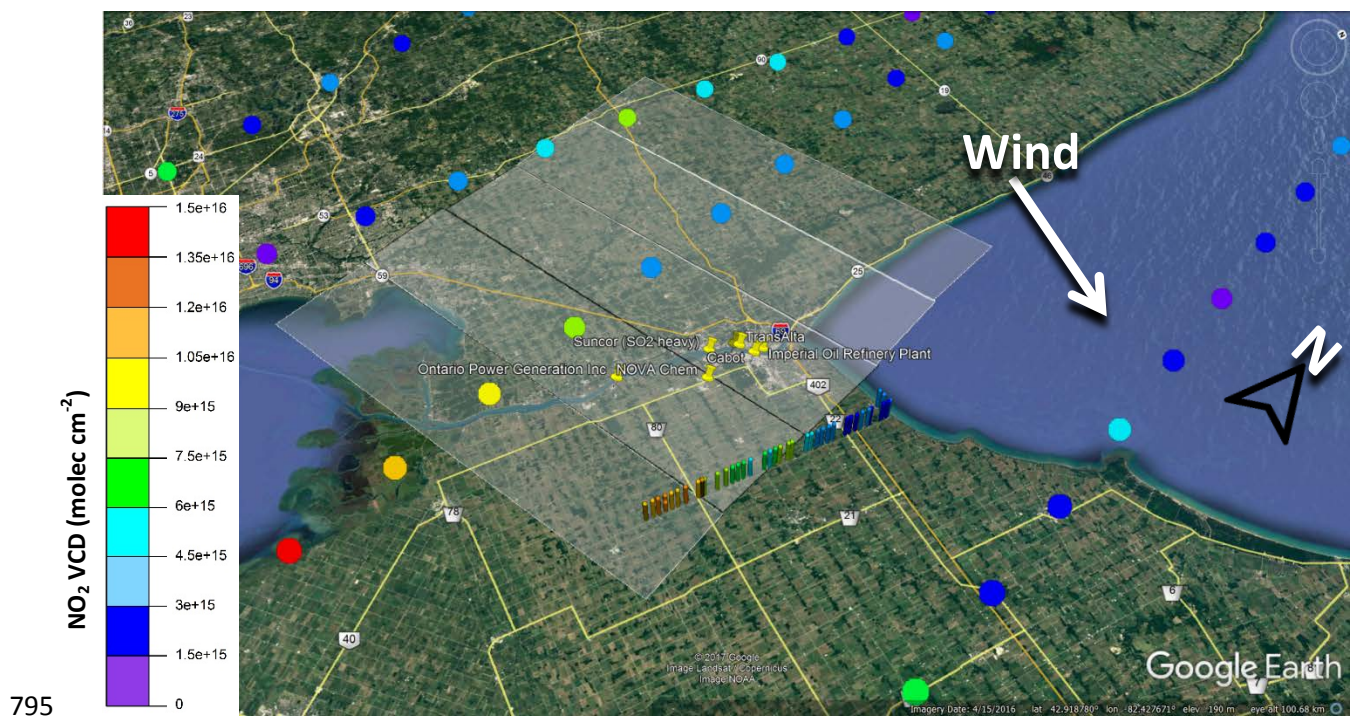
790

791

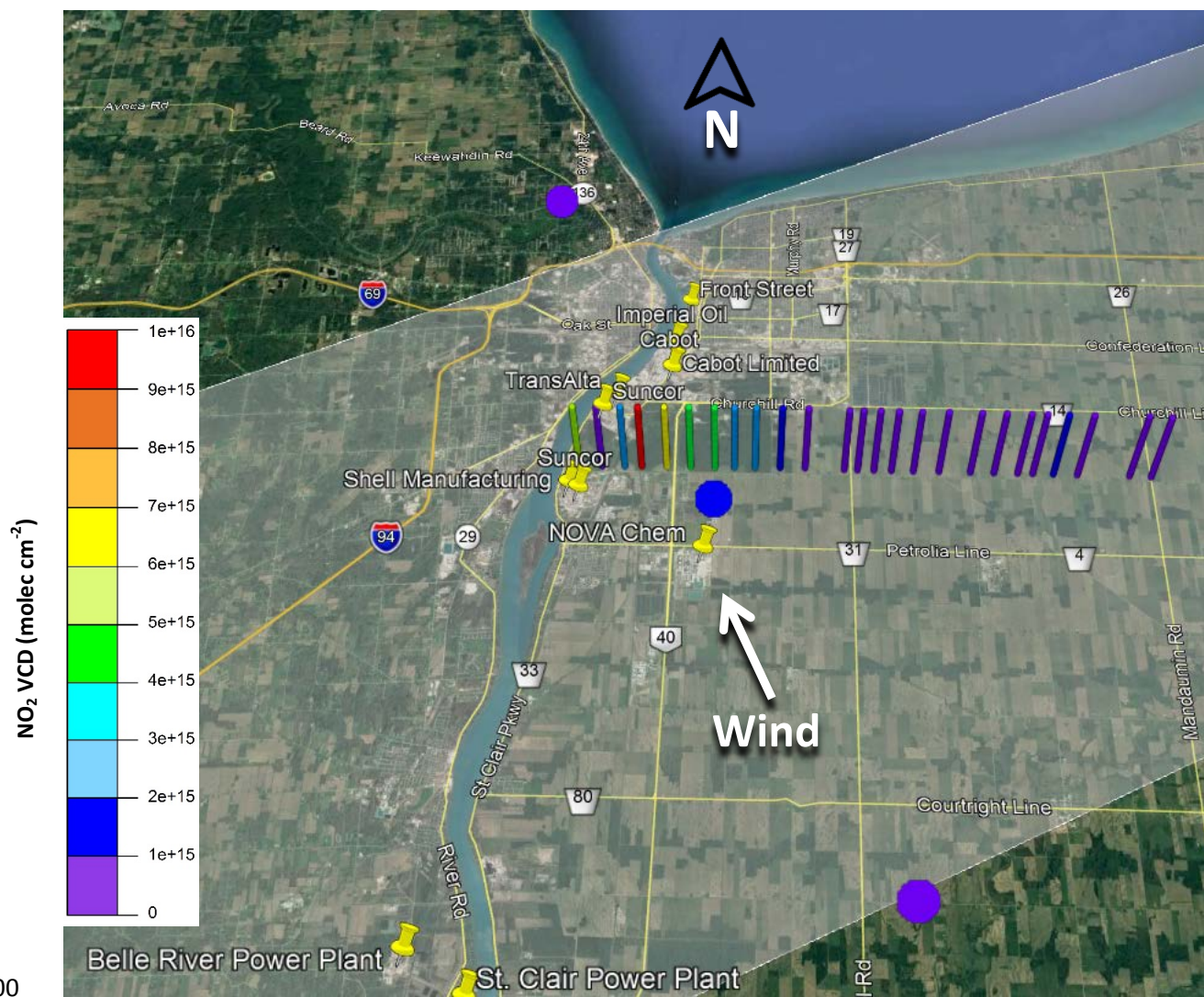


793 **Figure 9** SO₂ VCDs along route for emission estimate (Day 1 Route 3).

794



796 **Figure 10** Day 1 NO₂ VCDs from OMI satellite VCDs and mobile-MAX-DOAS Route 4. OMI satellite pixels
 797 closest to Sarnia were measured at ~18:00 local time. Semi-opaque rectangles centered on the colored dots
 798 (indicating satellite VCD value) indicate the spatial extent of the pixel.



800

801 **Figure 11** Day 3 NO₂ VCDs from OMI satellite and mobile-MAX-DOAS Route 1. OMI pixels shown were
 802 measured at ~18:00 local time. Semi-opaque rectangle centered on the colored dots indicates the spatial extent of the
 803 pixel.